FSC-ESD-217/89/448

MARS ROVER RTG STUDY

July 7, 1989

Principal Investigator & Author:

A. Schock

Contributors:

T. Hamrick
T. Or
V. Sankarankandath
M. Shirbacheh
E. Skrabek

FAIRCHILD
SPACE COMPANY
GERMANTOWN, MARYLAND 20874-1181

FSC-ESD-217/89/448

MARS ROVER RTG STUDY

July 7, 1989

Principal Investigator & Author:

A. Schock

Contributors:

T. Hamrick
T. Or
V. Sankarankandath
M. Shirbacheh
E. Skrabek

S-139.109 7-89C

MARS ROVER RTG DESIGN STUDY

Preface

This volume contains preprints of three papers to be presented at the 1988 Intersociety Energy Conversion Engineering Conference. These are the result of a Radioisotope Thermoelectric Generator (RTG) design study which the U.S. Department of Energy commissioned Fairchild Space Company to conduct in support of the Mars Rover and Sample Return mission study under study at the Jet Propulsion Laboratory:

A. Requirements and Designs for Mars Rover RTGs, by A. Schock and V. Sankarankandath of Fairchild Space Company and M. Shirbacheh of Jet Propulsion Laboratory.

B. Thermal and Electrical Analysis of Mars Rover RTGs, by A. Schock, T. Or, and E. Skrabek of Fairchild Space Company.

C. Structural Design and Analysis of Mars Rover RTGs, by A. Schock and T. Hamrick of Fairchild Space Company.

The three papers are interrelated. Each utilizes results from the other two. Paper B contains an addition that is not included in the conference proceedings.

A. Schock
July 5, 1989

CONTENTS

A. REQUIREMENTS AND DESIGNS

Introduction	A1
Background	A1
MRSR Objectives and System Elements	A2
Mars Rover Design	A3
RTG Requirements	A4
RTG Environment	A4
Design Approach	A5
Heat Source	A5
Thermoelectric Elements	A6
RTG Design Options	A6
Key Design Problem	A7
Baseline RTG Design	A7
Heat Source Support Structure	A8
Multicouple RTG	A9
Summary and Conclusions	A10

B. THERMAL AND ELECTRICAL ANALYSIS

Introduction	B1
Mass Breakdown of Baseline RTG	B1
Mass of Half-Length RTG	B2
Mass of Multicouple RTG	B2
RTG Thermal Environment	B3
Thermal and Electrical Analysis	B3
Temperature Distribution of Baseline RTG	B4
Axial Variation of Heat Flow Rates	B4
Axial Temperature Profiles	B5
Axial Voltage and Efficiency Profiles	B5
Effect of Cooling Mode on RTG Performance	B6

Effect of Lifetime on RTG Performance B6
Effect of RTG Length on Performance B7
Multicouple RTG Performance B7
Effect of Thermoelectric Material Properties
Materials Studied B8
Assumptions B8
Thermoelectric Analysis B9
Results and Conclusions B11

C. STRUCTURAL DESIGN AND ANALYSIS

Introduction C1
Structural Design C2
Required Preload and Resultant Stresses C3
Designing the Belleville Springs C6
Deformation and Stresses with Heat Source
Supported by Cantilevered RTG Housing C7
Summary and Conclusions C9

REQUIREMENTS AND DESIGNS FOR MARS ROVER RTGs

A. Schock, V. Sankarankandath
Fairchild Space Company, Germantown, MD

M. Shirbacheh
Jet Propulsion Laboratory, Pasadena, CA

ABSTRACT

The current-generation RTGs (both GPHS and MOD) are designed for operation in a vacuum environment. The multifoil thermal insulation used in those RTGs only functions well in a good vacuum. Current RTGs are designed to operate with an inert cover gas before launch, and to be vented to space vacuum after launch. Both RTGs are sealed with a large number of metallic C-rings. Those seals are adequate for retaining the inert-gas overpressure during short-term launch operations, but would not be adequate to prevent intrusion of the Martian atmospheric gases during long-term operations there. Therefore, for the Mars Rover application, those RTGs must be modified to prevent the buildup of significant pressures of Mars atmosphere or of helium (from alpha decay of the fuel). In addition, a Mars Rover RTG needs to withstand a long-term dynamic environment that is much more severe than that seen by an RTG on an orbiting spacecraft or on a stationary planetary lander. This paper describes a typical Rover mission, its requirements, the environment it imposes on the RTG, and a design approach for making the RTG operable in such an environment. Specific RTG designs for various thermoelectric element alternatives are presented.

INTRODUCTION

In December 1988 the Department of Energy's Office of Special Applications (DOE/OSA) asked Fairchild Space Company to investigate RTG (Radioisotope Thermoelectric Generator) design options for powering a Martian Rover vehicle. That vehicle is a critical part of the Mars Rover and Sample Return (MRSR) mission, which is under preliminary study by NASA's Jet Propulsion Laboratory (JPL) with the support of the Johnson Space Center (JSC). JPL is responsible for the overall MRSR study and, among other items, for the design of the Rover vehicle.

The MRSR mission also requires a lower-power RTG for its stationary lander. However, work on this was deferred in our study, because the basic solutions worked out for the more difficult Rover application will also be applicable to the less demanding stationary lander application.

The purpose of the DOE-sponsored Fairchild study is to support JPL and JSC by providing the mission planners with information about the RTG masses and sizes for various options of differing technology readiness. Its aim is to quantify the performance improvements achievable if new technologies are successfully developed, to provide our best estimates of the required time, effort, success probability, and programmatic risk in developing those new technologies, and thus to help identify the best strategy for meeting the MRSR system goals. In addition, the Fairchild study is useful in specifying critical design and operational requirements for integrating the RTG with the Rover and the launch vehicle (particularly cooling during orbit transfer), and in identifying what additional information JPL and JSC will need to furnish before the RTG design can be finalized. The various RTG design characterizations must be accurate and consistent, to permit meaningful comparisons among the different design options. The electrical, thermal, and structural analyses of the RTGs are described in companion papers presented at this conference [1, 2]

BACKGROUND

The long-term goal of the National Aeronautics and Space Administration is to expand human presence beyond earth and into the Solar System [3]. Mars, with its potential for eventual habitability, is targeted for human exploration and colonization. A manned mission to Mars must be preceded by robotic exploration of Mars, to bridge the gap between the knowledge gained by the 1976 Viking Mission and the knowledge required for a safe and effective human journey to Mars.

The Jet Propulsion Laboratory and Johnson Space Center are jointly studying such a mission, called Mars Rover Sample Return. That study is focused on understanding the system requirements and generating the first-order system design that meets these requirements [4]. The mission requires orbiters, landers and a Rover in Mars orbit and/or on the Mars surface.

RTGs have been selected as the primary power source for the surface elements of the MRSR system. They have a long and successful history of space flight, and their reliability and performance have been demonstrated in missions such as Pioneer, Viking, and Voyager [5]. The current-generation RTGs, however, are designed for space operation and must be modified for Mars surface operation.

MRSR OBJECTIVES AND SYSTEM ELEMENTS

The objective of the MRSR mission is to determine the geological, climatological and biological history of the planet Mars, and to characterize its near-surface materials. The mission will also provide information on the Mars environment, and test key technologies for human exploration of the planet. The mission objectives are achieved by making in-situ analyses and returning selected samples to Earth for extensive studies.

A spectrum of possible mission and system designs has been examined against the broad science requirements [6]. These missions, which varied in launch configuration, launch date, and the various elements that constitute the mission, have been narrowed down to a reference mission that consists of five system elements: an Imaging Orbiter (IO), Communications Orbiter (CO), Rover, Sample Return Orbiter (SRO) and Mars Ascent Vehicle (MAV). The reference MRSR mission scenario and mission time line currently envisioned by the project are summarized in Figures 1 and 2, respectively. As shown in Figure 1, the five system elements will be launched in four separate launch segments.

Figure 1. MRSR Reference Mission Scenario

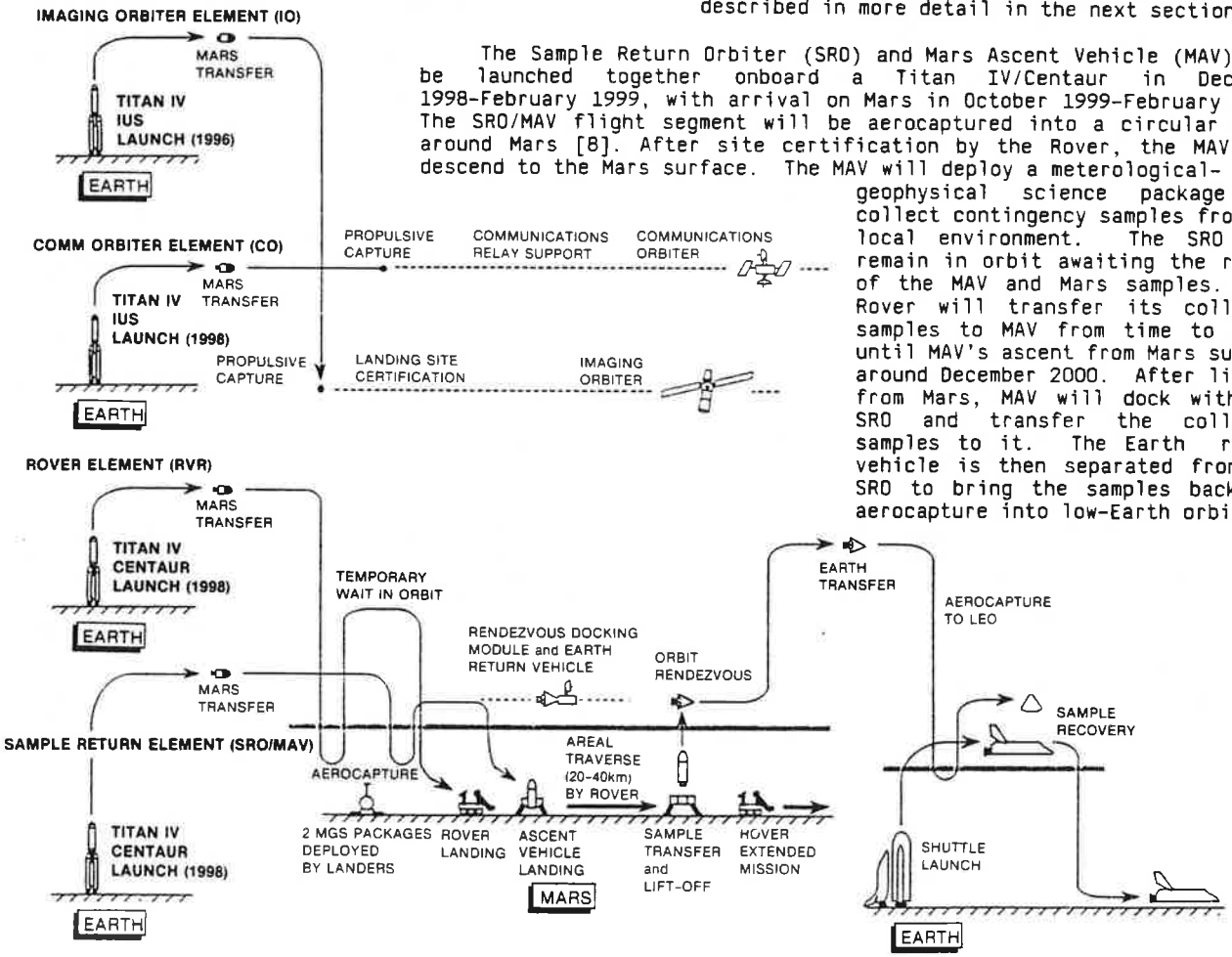

The Imaging Orbiter will be launched aboard a Titan IV/IUS in October-November 1996, with Mars arrival in August-October of 1997. It will map the surface of the planet for landing site selection and Rover Traverse Planning [7]. Nominally, the Imaging Orbiter will map sites within 39^{o} south or north of the equator. A total of ten 10 x 10 km sites will be mapped for selection of the landing site, and an area of 20 x 20 km at that site will further be mapped for Rover Traverse planning.

The Communication Orbiter will provide the communication link between the Mars surface elements and Earth [7]. It will be launched in November-December 1998 aboard a Titan IV/IUS, and will be placed in a stationary orbit such that the region between 65.7^{o} south and north of the equator is covered continuously. The Rover-to-Earth link is available at least 95% of every Mars Sol.

The Rover element will be launched aboard a Titan IV/Centaur in December 1998, with arrival at Mars in October 1999-January 2000. The Rover will traverse the surface of Mars, perform in-situ analyses, deploy science packages, select samples and return them to the ascent vehicle for delivery to Earth. Right after arrival, the Rover will also select a landing site for the MAV. The Rover design and its requirements are described in more detail in the next section.

The Sample Return Orbiter (SRO) and Mars Ascent Vehicle (MAV) will be launched together onboard a Titan IV/Centaur in December 1998-February 1999, with arrival on Mars in October 1999-February 2000. The SRO/MAV flight segment will be aerocaptured into a circular orbit around Mars [8]. After site certification by the Rover, the MAV will descend to the Mars surface. The MAV will deploy a meterological-geophysical science package and collect contingency samples from its local environment. The SRO will remain in orbit awaiting the return of the MAV and Mars samples. The Rover will transfer its collected samples to MAV from time to time, until MAV's ascent from Mars surface around December 2000. After liftoff from Mars, MAV will dock with the SRO and transfer the collected samples to it. The Earth return vehicle is then separated from the SRO to bring the samples back for aerocapture into low-Earth orbit.

Figure 2. MRSR Reference Mission Timeline

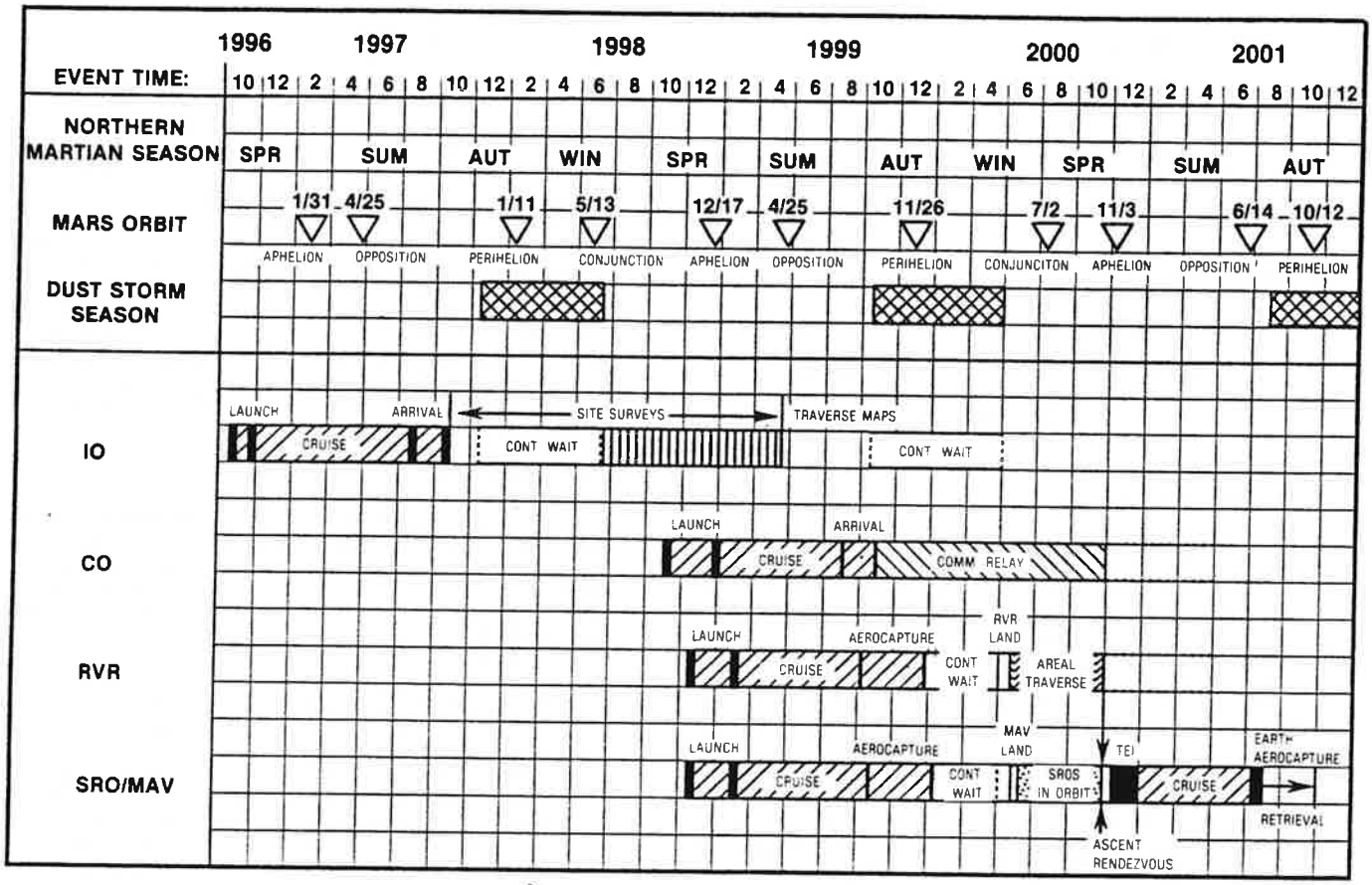

MARS ROVER DESIGN

The Rover element of the Mars Rover Sample Return mission for which the RTG study was performed is required to traverse more than 40 kilometers and collect 100 samples from several geologically distinct sites [9]. The Rover will be equipped with semi-autonomous navigation capability, which means it can compare its surroundings with a stored map of the orbital view obtained by the Imaging Orbiter, and plan and execute a local path toward a designated point. This autonomy greatly increases the Rover's range, since it reduces the need for frequent commands from Earth. Theoretically, the Rover can go several kilometers without requiring intervention from Earth.

A possible Rover mobility system is a six-wheeled pantograph, with one-meter wheels that can move across rough terrain. The Rover is further equipped with an imaging camera, multispectral imaging for science and navigation, optical microscope, spectrometers (alpha, proton, neutron, x-ray), electromagnetic sounders, gas analyzer, and differential scanning calorimeter. The sample acquisition by the Rover will be accomplished in several stages: remote sample characterization, location and designation of interesting samples, positioning and manipulation of the Rover to acquire the sample, and preserving the samples for return to the MAV.

The Rover will return with samples to the MAV several times, where each time the distance traveled will expand as the confidence in the Rover is increased. A typical activity pattern is depicted in Figure 3, and the Rover power requirements for a typical 1000-minute period are illustrated in Figure 4 [10].

Figure 3. Illustrative Rover Activity Patter

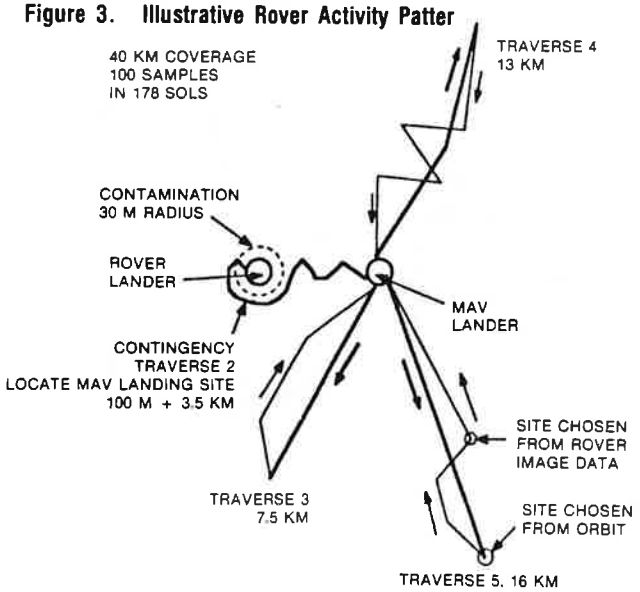

Figure 4. Power Demand Profile for Typical Mars Rover Activities

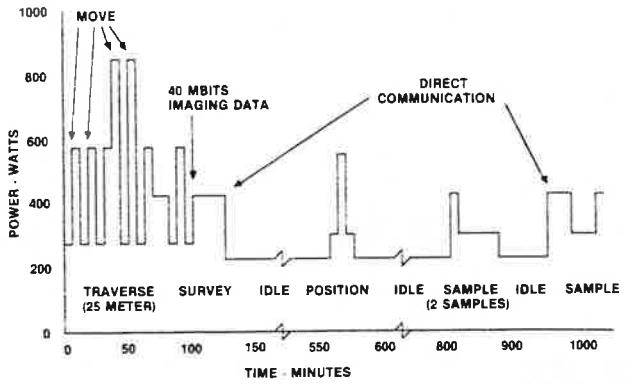

RTG REQUIREMENTS

The MRSR mission calls for the Rover to operate for four years after launch. The launch is assumed to occur three years after fuel encapsulation, and to be preceded by one year of full-temperature operation of the thermoelectric converters. Thus, by the end of the mission the RTG's fuel will have decayed for seven years, and its converters will have operated and degraded at full temperature for five years.

As illustrated in Figure 4, the Rover has an average power requirement of 500 watts, with peak power demands of over one kilowatt when the Rover is climbing a slope or in the process of sample acquisition. The RTGs will be designed to provide continuous power with an output of 500 watts at the end of mission, and these will be supplemented by rechargeable batteries for meeting the peaks of higher power demand. The high-power-density batteries will be recharged by the RTGs during the idle mode of the Rover.

Figure 5. Illustrative Rover Design with Four 125-Watt RTGs

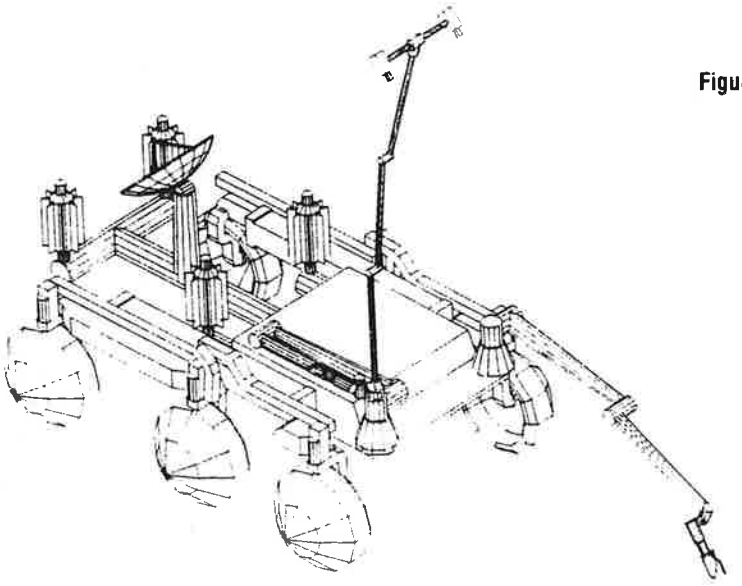

The number and location of RTGs on the Rover is very critical and require trade-off analysis. The Rover designers prefer several small RTGs distributed around the vehicle. This arrangement helps in the load distribution and also facilitates use of the RTGs' waste heat for thermal management of the Rover body and electronics bays. Also, shorter RTGs are less likely to block other Rover instruments and/or antennas. On the other hand, longer RTGs offer a higher specific power, because of decreased end losses and weights. They also are less likely to obscure the view of each other's radiators to space. At present, two concepts for integrating the RTGs with the Rover are undergoing evaluation, one employing two 250-watt RTGs, and one employing four 125-watt RTGs mounted on top of the Rover. The latter integration scheme is illustrated in Figure 5.

RTG ENVIRONMENT

Both the Rover and Mars environments present new challenges to the RTG designer. Previous RTGs (MHW, GPHS) were designed primarily for operation in microgravity and in a high vacuum after launch. The Rover and Mars environments are more difficult, mechanically, thermally, and atmospherically.

From the dynamic-environment point of view, the Rover RTG has to withstand launch, entry, landing, and traverse loads that occur at different times in the life of the mission. These loads cannot be accurately determined until the spacecraft and Rover structures are better defined. In the absence of such definition, the RTG design study was based on 3-axis design loads of 25 G during Earth launch and 15 G during and after Mars landing, for the duration of the Mission.

The Rover RTG also has to operate in a temperature environment that varies much more than that seen by most previous RTGs. During entry into the Martian atmosphere, the Rover-mounted RTGs are enclosed in a protective aeroshell, as illustrated in Figure 6. Therefore,

Figure 6. Rover with RTGs and Lander Enclosed in Aeroshell

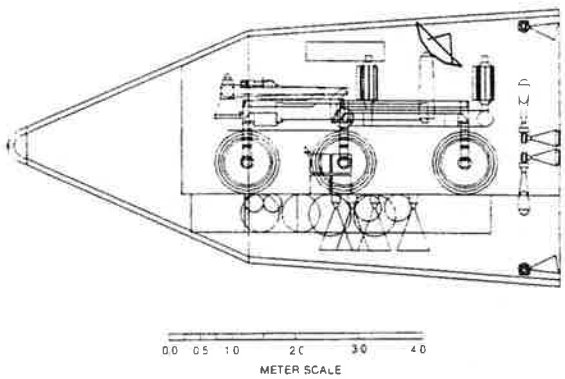

during Earth launch and cruise to Mars, the RTGs require an auxiliary cooling loop to transfer their waste heat to radiators. During Mars operation, when the RTGs are cooled by radiation, diurnal and seasonal temperature fluctuations cause their effective sink temperature to vary from a minimum of 140°K to a maximum of 300°K.

The most difficult problem imposed by Mars surface operations is the presence of an external atmosphere [11]. The thermoelectric converter elements in the RTG are embedded in multifoil thermal insulation, to minimize heat losses from the hot heat source to the cool generator housing. Thus, the insulation forces most of the heat through the thermoelectric legs.

Multifoil insulation performs well in the absence of conducting gases, but degrades rapidly when such gases are present. Moreover, at the projected operating temperatures even small amounts of some of the Martian gases would react with the converter's materials and degrade its performance. Therefore, the thermoelectric converter has to be sealed off from the Mars atmosphere and from the helium that is continuously generated by alpha decay of the isotope fuel.

DESIGN APPROACH

The first decision is the selection of the thermoelectric materials. The basic choice is between TAGS (Te-Ag-Ge-Sb) and SiGe (with or without GaP additives). TAGS was used on earlier missions, including the 1976 Viking mission to Mars. SiGe is used in all recent and current space RTGs, including LES-8/9, Voyager, Galileo, Ulysses, and the more advanced Mod RTG under development by DOE.

TAGS thermoelectrics operate at lower hot- and cold-junction temperatures than SiGe. Their hot-junction temperatures are far below the temperature capability of current radioisotope heat sources. Therefore they would not take proper advantage of that capability. SiGe elements come much closer to matching the heat source temperature limits.

TAGS thermoelectric elements have only been used in spring-loaded RTGs. Such RTGs tend to be much heavier than radiatively coupled RTGs, particularly since they use relatively bulky and inefficient fibrous insulation. By contrast, the thermoelectric elements in SiGe RTGs are heated radiatively. Thus, they do not contact the heat source, and no spring loading is required. They are insulated with lighter, more compact, and more efficient multifoil insulation.

Since TAGS elements operate with much lower hot-junction temperatures than SiGe, they also demand correspondingly lower cold-junction temperatures for efficient operation. This would require relatively large and heavy radiators. The lower cold-junction temperatures would be particularly disadvantageous in the present application, because they would make the RTG power output more sensitive to the large seasonal and diurnal temperature fluctuations on the Martian surface.

For these reasons, the Rover RTG design study is based on the use of SiGe rather than TAGS elements.

To minimize the need for new developments and allow the use of existing fabrication drawings and test fixtures, the initial design studies were conservatively based on: standard General Purpose Heat Source modules, which have been developed and safety-qualified for the Galileo mission; standard-size unicouples, developed and extensively lifetested for the Voyager and Galileo missions; standard-size multicouples, lifetested in DOE's Mod-RTG program; and thermoelectric performance parameters and degradation rates that have been demonstrated in extended tests of SiGe unicouples and SiGe/GaP multicouples.

HEAT SOURCE

DOE has spent approximately ten years and $40-50M on the development [12] and safety qualification [13] of the General Purpose Heat Source (GPHS), for initial deployment on the Galileo and Ulysses space exploration missions. As a result of that effort, this heat source is extremely well characterized, much more so than radioisotope heat sources used on previous space missions.

The heat source is modular, and a sectioned view of a standard 250-watt module is shown in Figure 7. Each GPHS module contains passive safety provisions against fuel release for all credible accident conditions. As shown, each module contains four iridium-clad $Pu^{238}O_2$ fuel capsules surrounded by graphitic components, including an aeroshell designed to withstand reentry ablation, a thermal insulator to avoid excessively high clad temperatures during the reentry heat pulse and excessively low clad temperatures at earth impact, and an impact shell to help absorb impact energy and reduce fuel capsule deformation during earth impact. Viewed from the outside, each GPHS module is a graphite brick of roughly 2 x 4 x 4 inches. This module was used as the building block for all RTG designs presented in this paper and its companions [1, 2].

Figure 7. General-Purpose Heat Source Module (250 Watt)
Sectioned At Midplane

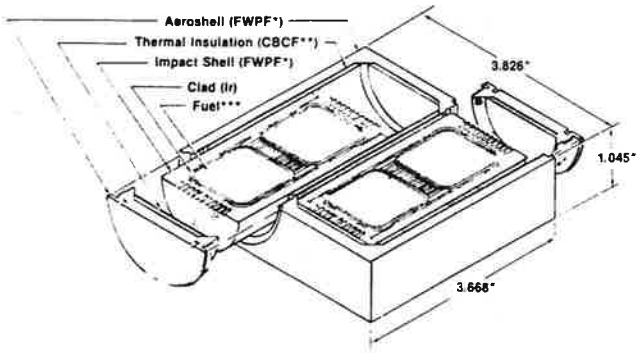

*Fine-Weave Pierced Fabric, a 90%-dense 3D carbon-carbon composite
**Carbon-Bonded Carbon Fibers, a 10% dense high-temperature insultor
***62.5-watt $^{238}PuO_2$ pellet

THERMOELECTRIC ELEMENTS

The present study is based on two alternative types of thermoelectric (TE) elements: unicouples and multicouples. Both use SiGe-based thermoelectric materials. The standard unicouple, which was used in the MHW RTGs flown on the Voyager and LES 8/9 missions and in the GPHS RTGs for the Galileo and Ulysses missions, is depicted in Figure 8. The P and N legs are 0.8" long, and the 1"-square hot-shoe collects the heat radiated by the heat source and delivers it to the TE legs. The cold end of the unicouple is bolted to the RTG housing, and the electrical connections between couples are made on the inside of the housing.

Figure 8. Unicouple

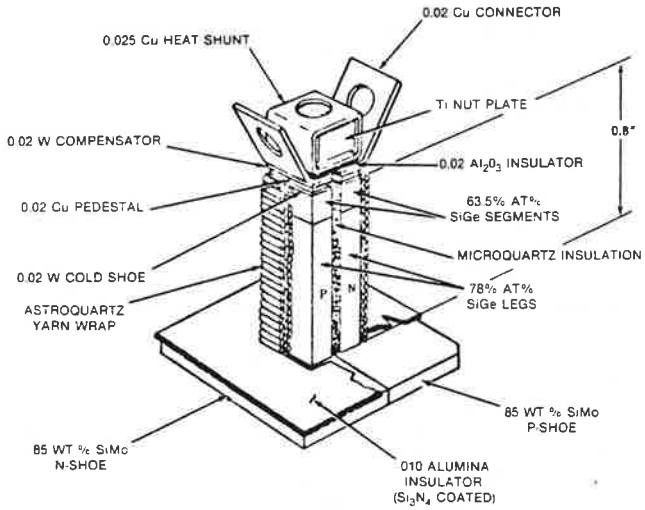

The standard multicouple, developed for the Mod-RTG, is depicted in Figure 9. It differs from the unicouple primarily in that instead of two TE legs each TE element has 40 legs, which together with its hot and cold electrodes form 20 series-connected couples. The standard multicouple legs are only 0.3" long, compared to the unicouple's 0.8" leg length. This reduces the weight of the thermal insulation and of the RTG housing.

Figure 9. Multicouple Cross-Section

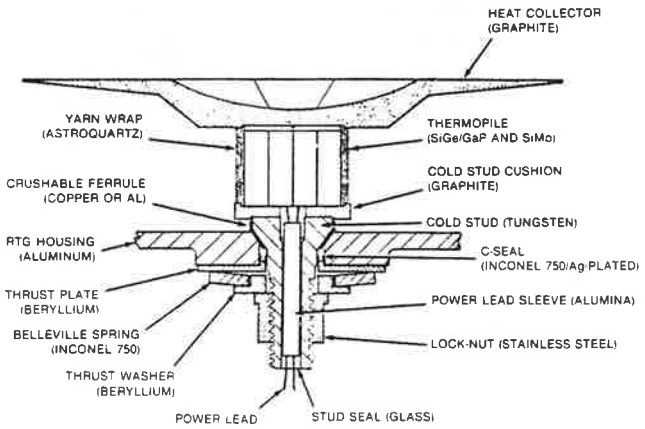

The multicouple's legs are bonded to, and insulated from, each other by 0.002" glass layers. The heat collector, approximately 2" square, is made of graphite. In contrast to the unicouple, the multicouple's mounting stud and power leads penetrate through the RTG housing, and electrical connections between multicouples are made on the outside of the housing. As will be seen, these differences affect the Rover RTG design.

RTG DESIGN OPTIONS

Initial RTG designs were conservatively based on standard unicouples and multicouples, using demonstrated thermoelectric performance levels and degradation rates. The standard unicouples and multicouples are the only SiGe TE elements for which an extensive experimental data base exists. Large assemblies of SiGe unicouples have been used in RTGs for a number of flight missions (LES 8/9, Voyager, Galileo, Ulysses), and have demonstrated stable performance with moderate and predictable degradation rates for periods in excess of 100,000 hours.

Multicouples operating at the required hot-junction temperature (1000°C) have a much smaller data base. Their development was initiated in the late 1970s [14], their present design was defined in 1983 [15], and their most successful test to date (of an assembly of eight multicouples) was a 6000-hour run at Fairchild completed in December 1988, when it was temporarily interrupted for a planned modification of the test fixture and for withdrawal of three of the multicouples for destructive examination..

During the 6000-hour test, the six multicouples that operated with a positive bias with respect to the RTG housing exhibited very stable performance, but the two multicouples that were negatively biased exhibited unacceptable degradation rates. This negative-bias problem had been first identified by Fairchild tests more than two years earlier. Although GE has been working diligently to solve the problem, the solution is not yet in hand. Until it is, they can only be used if all multicouples in the RTG are positively biased. Fortunately, the RTG can be configured to achieve that condition, albeit at some mass penalty.

Beyond the standard unicouple and multicouple, a number of RTG designs based on more advanced thermoelectric elements were also defined and analyzed. The postulated advances were in element geometry and/or in material performance. They ranged from relatively minor changes to major advances. For the most advanced option, there is no experimental basis nor clear development pathway. It was included in the study to define the possible performance benefits if the postulated advances were in fact achieved.

Detailed descriptions of the advanced design options and the resultant performance improvements are presented in the next paper [1] in these proceedings. This summarizes and discusses the results of the thermal, thermoelectric, and electrical analyses of the

various design options. The present paper deals primarily with the basic design approach, which is the same for all of the design options. Thus, the two basic designs described in this paper apply to all options of interest.

KEY DESIGN PROBLEM

The key problem in designing an RTG for Mars is the need to vent the helium generated by the fuel's alpha decay to the outside without allowing the Martian atmosphere to enter into and build up harmful quantities within the RTG. In the 1976 Viking mission to Mars, the 35-watt RTGs used fibrous insulation, which is much less effective than multifoil and leads to a substantially higher system mass. However, the more efficient and compact multifoil insulation used in the present study is only effective in a good vacuum (<1 torr). But the existing GPHS-RTG and Mod-RTG both use a large number of metal C-ring seals. Such seals are adequate for retaining the inert cover gas during the short launch period, but not for preventing intrusion of the Martian atmosphere during extended Mars operations.

To prevent helium pressure buildup inside the RTG above 1 torr, the use of a selective vent has been considered. But to maintain an internal helium pressure of less than one torr, such a vent would have to have a very low flow resistance. However, a low-flow-resistance vent would allow appreciable back diffusion of Martian gases into the RTG. This would be unacceptable unless these Martian gases were effectively gettered as soon as they entered the RTG. Even small quantities of Martian gases (CO_2, CO, O_2) would result in deleterious reaction with the RTG materials.

Since the system of selective vent and effective getter has not yet been demonstrated, the present study is based on RTG designs with an evacuated annular converter, sealed off from the both the internal helium and the external Mars atmosphere, as illustrated in the next figure.

BASELINE RTG DESIGN

Figures 10 and 11 show cross-sectional views at different locations of the baseline RTG. Figure 10 shows two horizontal sections (AA and BB) and Figure 11 shows a vertical section (CC). Section AA shows a horizontal cut through the active region of the RTG, i.e., through the midplane of a heat source module and through the midplane of a ring of thermoelectric unicouples. The rest of Figure 10 represents Section BB. It shows a horizontal cut through the upper and lower heat source support structure. The locations of Sections AA and BB are indicated in Figure 11.

Figure 11 shows a vertical cross-section (CC) of the RTG. As indicated in Figure 10, the left half of section CC shows a section that is perpendicular to the axes of the fuel capsules in the heat source stack and through two columns of thermoelectric unicouples mounted on the housing; and the right half of Section CC shows a diagonal cut through the heat source stack. The location of Section CC is shown in Figure 10.

In Figures 10 and 11 two different shading patterns are used to designate the helium volume inside the heat source canister and the Martian atmosphere outside the RTG housing. The intervening annular converter is evacuated, and is separated from the helium by the heat source canister and from the Martian atmosphere by the RTG housing.

Figure 10. Baseline RTG, Horizontal Cross-Section (B-B)

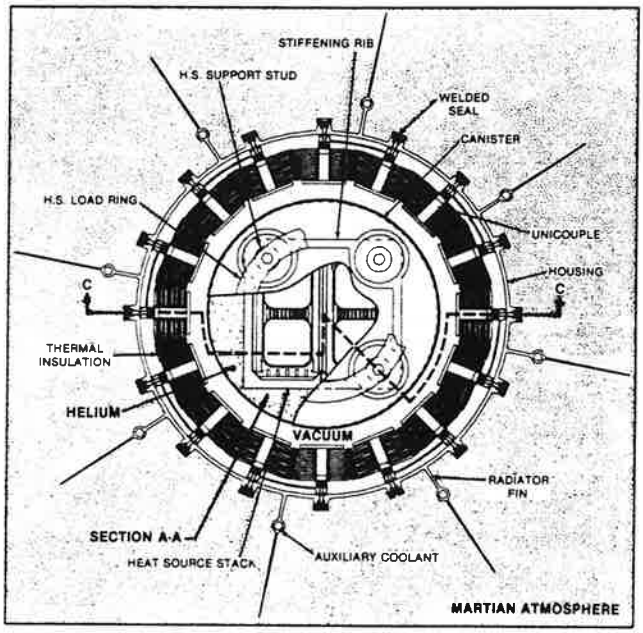

Figure 11. Baseline RTG, Vertical Cross-Section (C-C)

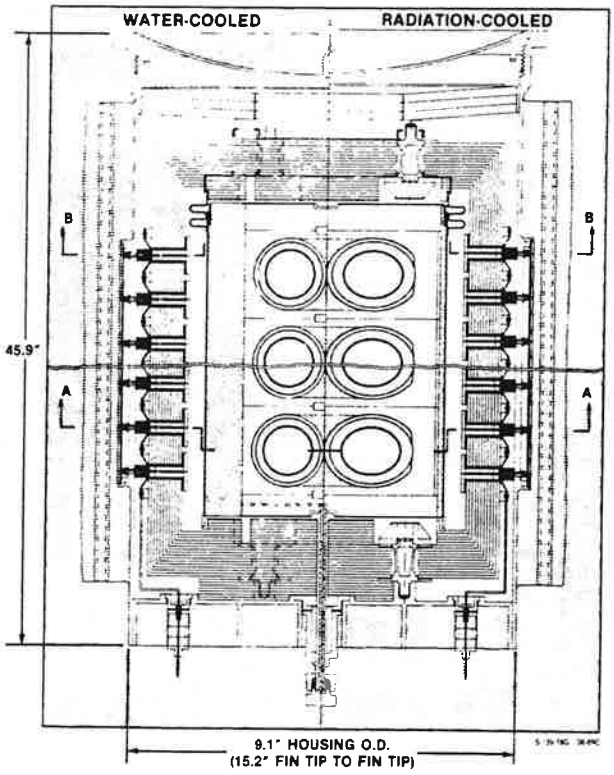

Figure 10 shows that, as in the Galileo RTG, there are 16 unicouples around the circumference, and these are bolted to the housing at 22.5° intervals. In the Galileo RTG the mounting bolt holes of its 572 unicouples are sealed by metal C-rings, but these would be inadequate for preventing inflow of the Martian atmosphere over mission life. In the present design, the bolt holes are hermetically sealed by 16 aluminum cover strips welded to the aluminum housing ribs.

The heat source of the 250-w(e) baseline RTG consists of a stack of 18 GPHS modules, but for improved visibility only three are depicted in Figure 11. As seen, there are two rings of 16 unicouples for each of the 18 heat source modules, for a total of 576 unicouples per RTG. As shown, the baseline RTG has a height of 45.9", a housing diameter of 9.2", and a radiator tip-to-tip span of 15.2".

The unicouples in the baseline RTG are embedded in a 0.8"-thick layer of thermal insulation, consisting of 60 alternating layers of 0.0003"-thick molybdenum foil and quartz cloth. This type of insulation, which was used in the MHW and Galileo RTGs, is considerably heavier than multifoil insulation with zirconia-particle spacers used in the Mod-RTG.

As in the Galileo RTG, there are eight radiator fins and each fin contains an auxiliary cooling tube. The auxiliary coolant is used to control the RTG housing temperature during launch and during transit to Mars, while the RTG is enclosed in the aeroshell that protects the Rover and lander during their entry into the Martian atmosphere. After entry, the aeroshell is jettisoned, the auxiliary cooling is discontinued, and the RTG is cooled primarily by radiation from the fins. Convective cooling by the Martian atmosphere, even on a cold windy day, makes only a relatively minor contribution to heat rejection.

The trapezoidal radiator fins shown in Figure 10 have a root thickness of 0.066", a tip thickness of 0.015", and a root-to-tip height of 3". These dimensions are merely illustrative. The optimum fin dimensions will be determined by a detailed radiator design optimization, described in companion papers [1, 2] in these proceedings.

Figure 11 shows the series connections between the unicouples and the RTG terminals at the bottom of the converter. As shown, the RTG requires bimetallic joints from aluminum to stainless steel and to Kovar. Such bimetallic joints have been formed by explosive bonding, and have undergone extensive thermal-cycling tests. Their small diameter should enhance their reliability. The Kovar-alumina-Kovar metal-ceramic seals form the feedthroughs for the electrical terminals. Figure 11 also depicts the vent tube and Viton seal through which the helium from the canister is vented to the Martian atmosphere.

As mentioned earlier, the baseline RTG has 36 rings of 16 unicouples, or a total of 576 unicouples. The 576 couples are connected in two identical (180-degree) series-parallel networks, as illustrated in Figure 12. There are 144 couples in series, to generate the desired 30-volt output. The couples in each network are parallel-connected in groups of two, to enable the RTG to continue operation in case of single-point failures. Alternatively, the 576 couples could be connected in a single 144 x 4 series-parallel network for even higher reliability.

Figure 12. Schematic Circuit Diagram of Baseline RTG

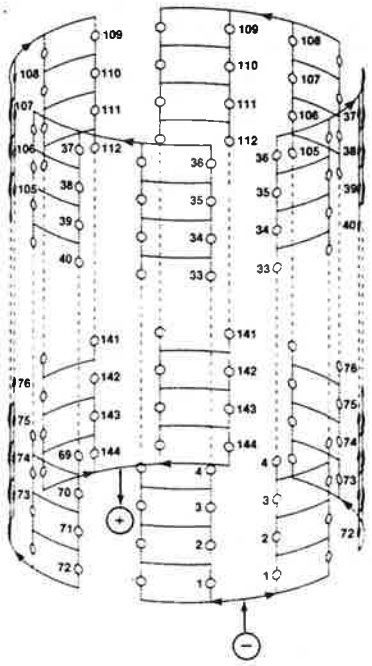

HEAT SOURCE SUPPORT STRUCTURE

One of the most critical issues in designing an RTG with stacked heat source modules is the scheme for supporting that stack. The modules must stay together during transverse G-loads. But for safety reasons, it is desired that the modules separate during reentry, to obtain a low impact velocity. The method of achieving this in the Rover RTG is illustrated in Figure 10 and 11.

The heat source stack is only supported at its ends, and a large (5500-lb) axial preload is required to hold the stack together during launch under the assumed 25-G transverse load. The axial preload is applied directly to the ends of the stack, via the canister's end caps. The canister's side wall plays no structural role; it is merely a helium container, and is thin enough to burn off during reentry.

The lateral support and axial preload force on the heat source is applied at each end of the canister by a set of four low-conductance Inconel studs and zirconia insulators, similar to those used in the Galileo RTG. Two of the eight studs are visible in the diagonal cross-section, at the right of Figure 11. As shown in Figure 10, each of the canister's end caps contains an integral square structure. These serve to stiffen the end caps and to spread the axial load from the four

support studs to the four edges of the heat source stack. As indicated in the left half of Figure 11, the square load-spreading structure employs four 1"-high stiffening ribs.

The tops of the four studs are bolted to a titanium load ring, which is laterally supported and axially loaded by a set of three nested Belleville springs made of 0.2"-thick titanium. Three springs are used in order to generate the required preload without exceeding the allowable stress in the springs. The I.D. of the bottom spring bears against the load ring, and the O.D. of the top spring bears against a titanium set ring that is threaded to the I.D. of the aluminum housing. After the load is set, rotation of the set ring is prevented by pins protruding from the RTG's aluminum cover. That cover serves only as a pressure dome, and has no other structural function.

The support structure at the bottom of the heat source stack uses an identical set of Inconel studs and zirconia insulators. But there are no springs, and the studs are mounted directly on the RTG's aluminum base plate. The base plate employs 1"-high radial and circumferential ribs to supply the required stiffness.

Clearly, the heat source stack is ultimately held together by the RTG's low-melting aluminum housing. When that housing and the thin canister burn away during reentry, the heat source modules are free to disperse and impact individually.

The Belleville springs must supply sufficient force to enable the heat source stack to withstand the lateral G-loads during launch while the RTG fins are water-cooled. Once the Rover aeroshell is discarded after entry into the Martian atmosphere, the RTG is cooled radiatively for the balance of the mission.

When changing from water-cooling to radiation cooling, the RTG housing temperature rises about 100°C (on a summer day). This causes a differential growth of about 0.100" in the length of the high-expansion aluminum housing relative to the low-expansion graphite heat source stack, with a corresponding increase in the Belleville spring length and drop in spring force. In RTGs for other missions, the magnitude of the spring force is only important briefly during launch. In the case of the Rover RTG, the springs must still provide sufficient force after relaxation to hold the heat source together during Mars traverses for the balance of the mission.

The left half of Figure 11 depicts the water-cooled RTG during launch and transit to Mars, assuming a wall temperature of 100°C for the auxiliary coolant tubes. The right half of the figure depicts the radiatively cooled RTG on a hot Martian day. The top of the figure depicts the differential thermal growth and the resultant spring relaxation. The springs were designed to provide the axial forces required to resist lateral loads of 25 G during launch and 15 G on Mars.

MULTICOUPLE RTG

Horizontal and vertical cross-sections of an RTG employing standard-size multicouples are shown in Figures 13 and 14. The multicouple-RTG design depicted in those figure are generally similar to the unicouple-RTG design shown in the analogous Figures 10 and 11, and only the significant differences will be mentioned.

Figure 13. Multicouple RTG, Horizontal Cross-Section (B-B)

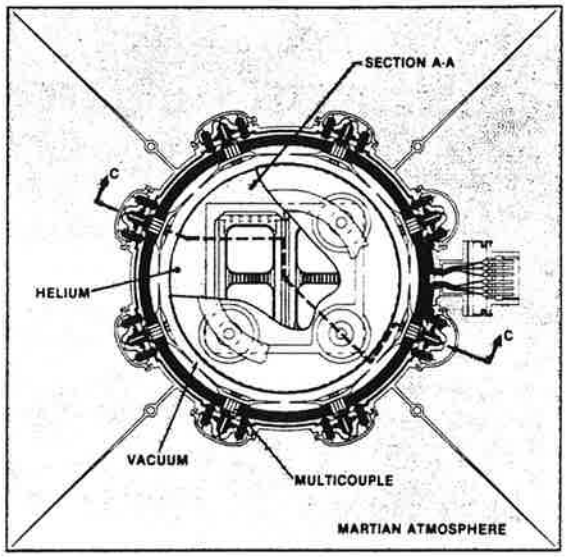

Figure 14. Multicouple RTG, Vertical Cross-Section (C-C)

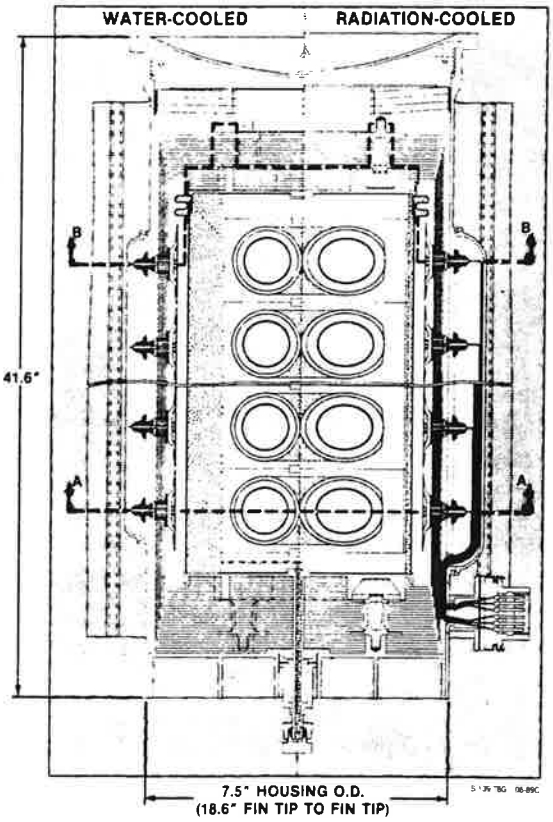

As in the Mod-RTG, there are eight multicouples per horizontal ring, and only one multicouple ring per heat source module. For a 250-watt(e) power output, the RTG has 16 heat source modules. Thus, there are 128 multicouples per RTG, or 22% as many TE units as in the unicouple RTG.

In the Mod-RTG the multicouple mounting holes are sealed by conical metal ferrules, but these would be inadequate for preventing inflow of the Martian atmosphere during long-term operations on Mars. Therefore, the bolt holes in the present design are hermetically sealed by eight semi-cylindrical aluminum seal covers welded to the aluminum housing hubs.

In the standard multicouple design, the leads pass through the housing wall, and are series-connected on the outside. To preserve hermeticity in the present RTG design, the series leads are passed back to the inside of the housing via insulated studs, for internal series connections between the eight multicouples in each ring.

As in the Mod RTG, the eight multicouples are embedded in a 0.3"-thick layer of thermal insulation, consisting of 60 layers of 0.0003"-thick molybdenum foils, separated from each other by zirconia spacer particles. This type of insulation is not only lighter than the standard unicouple insulation, but its lower thickness also leads to significant weight saving due to the consequent reduction (from 9" to 7.5") in housing diameter.

The option shown in Figure 13 has four radiator fins. The alternative of eight fins was also analyzed. The analytical results showed that the 8-fin option yields a higher specific power.

The series connections between thermoelectric elements are horizontal rather than vertical. The multicouple RTG design is modular [14], because each horizontal ring produces the desired RTG voltage (30V). Multicouples have operated stably for 6000 hours, before the tests was interrupted for fixture modification. But stable operation was only achieved when the multicouples were at a positive bias with respect to the RTG housing. Therefore, the Rover RTG is designed for positive bias operation of all multicouples. To avoid the possibility of single-point failures, this requires that the leads from each of the sixteen current loops be separately brought out to the power conditioning unit through a multipin terminal, as shown at the right of Figures 13 and 14.

SUMMARY AND CONCLUSIONS

The current multifoil-insulated GPHS-RTG and Mod-RTG designs can be modified to operate in an environment with an external atmosphere (e.g., Mars). This can be done while the helium generated by the fuel's alpha decay is vented to the external atmosphere. The use of novel selective vents and high-capacity getters is not required. The Rover RTGs can be built from standard and proven GPHS modules and standard SiGe unicouples or SiGe/GaP multicouples, using demonstrated thermoelectric material performance parameters. Rover's 500-watt power requirement can be satisfied with two 250-watt or four 125-watt RTGs, whose sizes are compatible with currently envisaged Rover designs. An auxiliary cooling loop (e.g., water and antifreeze) will be required to cool the RTG while it is within the Rover's aeroshell during launch and transit to Mars.

As in present RTGs, the modular heat source stack in the Rover RTG is held together by axial load springs. The Rover RTGs do not require mid-span supports. The Belleville load springs are designed to hold the heat source together in the water-cooled RTG under 25-G loads during Earth launch and Mars entry, and in the radiation-cooled RTG under 15-G loads during subsequent Mars operations. Basic designs have been prepared for both unicouple RTGs and multicouple RTGs. These designs apply both to current TE elements and to elements of advanced designs and materials.

Detailed analyses to compare the RTG mass and performance for a variety of designs and thermoelectric materials properties are described in companion papers [1, 2] presented at this conference. The principal conclusions derived from the results are:

- The baseline RTG has a mass of 63.2 kg, with a power output of 278 watts BOM and 256 watts EOM when radiating to a 300°K Mars environment.
- The baseline RTG has a BOM/EOM system efficiency of 6.32/6.01%, and a specific power of 4.74/4.37 watts/kg.
- The combined effect of fuel decay and thermoelectric material degradation during the four-year mission reduces the power output by 8%.
- The RTG can deliver full operating power during its water-cooled cruise to Mars.
- The power output of the radiatively cooled RTG is essentially independent of the Martian temperature.
- The mass of four 125-watt RTGs is 6% higher than that of two 250-watt RTGs.
- The specific power of the four 125-watt RTGs is 7% lower than that of the two 250-watt RTGs.
- The 250-watt baseline RTG has a length of 45.9 inches, and the 125-watt unit has a length of 41.6 inches. Either length appears to be compatible with currently envisaged Rover designs.
- A 250-watt RTG using standard multicouples is 23% lighter, 9.4% shorter, 7% more efficient, and has a 23% higher specific power than the baseline RTG using standard unicouples.

- The RTGs' fuel loading and mass can be significantly reduced by employing thermoelectric materials with higher figures of merit, when these become available.

The ultimate design and material selections will represent a trade-off between minimizing the RTG mass, to help meet the Rover system design goals of NASA/JPL, and minimizing the need for new technology, to reduce the development costs and programmatic risks of DOE.

REFERENCES

[1] A. Schock, T. Or and E. Skrabek, "Thermal and Electrical Analysis of Mars Rover RTGs." 24th Intersociety Energy Conversion Engineering Conference, 6-11 August, 1989.

[2] A. Schock and T. Hamrick, "Structural Design and Analysis of Mars Rover RTGs." 24th Intersociety Energy Conversion Engineering Conference, 6-11 August, 1989.

[3] Statement before the Committee on Energy and Natural Resources, United States Senate by Dr. Robert Rosen, Sept. 13, 1988.

[4] J.D. Bourke, J.H. Kwok, A. Friedlander, "Mars Rover Sample Return Mission." AIAA-89-0417, 27th Aerospace Science Meeting January 9-12, 1989, Reno, Nevada.

[5] G.L. Bennett, J.J. Lombardo and B.J. Rock, "Development and Use of Nuclear Power Sources for Space Applications." Journal of the Astronautical Sciences, Vol. XXXIX, Dec. 1981.

[6] J.T. Rose, "Conceptual Design of the Mars Rover Sample Return System." AIAA-89-0418, 27th Aerospace Science Meeting, January 9-12, 1989, Reno, Nevada.

[7] J. Randolph, "Mars Rover Sample Return Orbiter Design Concepts." AIAA-89-0421, 27th Aerospace Science Meeting, January 9-12, 1989, Reno, Nevada.

[8] T. Gamberk, L. Rogers, "Aerocapture, Entry and Landing Systems for the Mars Rover Sample Return." AIAA-89-0422, 27th Aerospace Science Meeting, January 9-12, 1989, Reno, Nevada.

[9] D. Pivirotto, T. Penn, W.C. Dias, "Mars Rover 1988 Concepts." AIAA-89-0419, 27th Aerospace Science Meeting, January 9-12, 1989, Reno, Nevada.

[10] "Mars Rover, Phase-1 Design Data Book", edited by B.K. Muirhead, Jet Propulsion Laboratory, April 23, 1988.

[11] "Environment of Mars, 1988", Jet Propulsion Laboratory, TM100470, Oct. 1988.

[12] A. Schock, "Design Evolution and Verification of the General Purpose Heat Source." Proceedings of the 1980 Intersociety Energy Conversion Engineering Conference, Volume 2, pages 1032-1042.

[13] G. Bennett, et al, "Update to the Safety Program for the General Purpose Heat Source Radioisotope Thermoelectric Generator for the Galileo and Ulysses Missions." Transactions of the Sixth Symposium on Space Nuclear Power Systems, Albuquerque, New Mexico, 8-12 January 1989.

[14] A. Schock, "Modular Isotopic Thermoelectric Generator." Proceedings of the 1981 Intersociety Energy Conversion Engineering Conference, Volume 1, pages 327-342.

[15] A. Schock, "Revised MITG Design, Fabrication Procedure, and Performance Predictions." Proceedings of the 1983 Intersociety Energy Conversion Engineering Conference, Volume 3.

ACKNOWLEDGEMENTS

The above work was supported by the U.S. Department of Energy's Office of Special Applications.

THERMAL AND ELECTRICAL ANALYSIS OF MARS ROVER RTGs

A. Schock, T. Or, E. Skrabek
Fairchild Space Company, Germantown, MD

ABSTRACT

The RTG designs described in the preceding paper in these proceedings were analyzed for their thermal and electrical performance. Each analysis consisted of coupled thermal, thermoelectric, and electrical analyses, using Fairchild-generated specialized computer codes. These were supplemented with preliminary structural and mass analyses. For each design, various cases representing different operating conditions (water-cooled/radiation-cooled, BOM/EOM, summer/winter, day/night) and different thermoelectric performance assumptions (from conservative to optimistic) were analyzed; and for every case, the heat flow rates, temperatures, and electrical performance of each layer of thermoelectric elements and of the overall RTG were determined. The analyses were performed in great detail, to obtain accurate answers permitting meaningful comparisons between different designs. The results presented show the RTG performance achievable with current technology, and the performance improvements that would be achievable with various technology developments.

INTRODUCTION

The preceding paper [1] in these proceedings described generic designs of RTGs to power the Mars Rover vehicle of the Mars Rover Sample Return (MRSR) mission under study at JPL. Two specific designs were described: one based on standard unicouples, large assemblies of which have demonstrated stable performance in very lengthy space and ground operations (>100,000 hrs); and one based on standard multicouples, which have demonstrated stability in much shorter tests (6000 hrs). The basic design concepts described in that paper are also adaptable to thermoelectric elements containing a variety of geometric and materials improvements.

The present paper presents mass breakdowns and describes detailed thermal, thermoelectric, and electrical analyses of both 250-watt and 125-watt RTG designs employing standard unicouples and demonstrated materials properties . It then proceeds to apply the same analyses to RTG designs employing thermoelectric elements of postulated advanced geometries and/or materials. Its purpose is to define the RTG parameters achievable with current technology, and to determine how much those parameters could be enhanced if various items of new technology could be successfully developed. When this information is coupled with an assessment of the difficulty, cost, and success probability of developing those items of new technology, it provides a basis for informed decisions about optimum program strategy for given schedule and budget limits.

MASS BREAKDOWN OF BASELINE RTG

The "baseline" Mars Rover RTG design is described in the preceding paper [1], and depicted there in Figures 10 and 11. It contains eighteen General Purpose Heat Source (GPHS) modules and 576 standard unicouples. It is designed for a nominal power output of 250 watts EOM, based on demonstrated thermoelectric performance levels. Its mass breakdown, based on a non-optimized radiator fin design, is presented in the left half of Table 1. The right half of the table shows the corresponding breakdown for the existing Galileo RTG, to ensure that all required RTG components have been properly accounted for in the Rover RTG mass breakdowns.

Table 1. Mass of Baseline RTG Versus Galileo RTG

RTG MASS BREAKDOWN (kg)	ROVER RTG BASELINE DESIGN		GALILEO RTG	
HEAT SOURCE (33.8/30.1kg)				
GPHS MODULES (18/18)		26.05		26.05
FUEL (PuO_2)	10.73		10.73	
CAPSULES (Ir)	4.21		4.21	
GRAPHITICS	11.11		11.11	
H.S. CANISTER (Mo)		3.77		0.00
SIDE WALLS	2.21		----	
BELLOWS	0.11		----	
END CAPS AND LOAD SPREADERS	1.45		----	
H.S.STRUCTURAL SUPPORTS		3.94		4.05
GRAPHITE PRESSURE PLATES	0.52		0.53	
LOAD STUDS+ZIRCONIA	0.27		0.38	
BELLEVILLE SPRINGS (Ti)	2.31		0.51	
OTHER PRELOAD HARDWARE	0.84		1.69	
MID-SPAN SUPPORT ASSEMBLY	----		0.94	
CONVERTER (24.9/26.0kg)				
ELECTRICAL CIRCUITS		7.74		7.65
TE ELEMENTS (576/572)	5.43		5.40	
TE FASTENERS AND SEALS	1.09		1.08	
ALUMINA INSULATORS	0.88		0.88	
ELECTR. CONNECTORS + TERMINALS	0.34		0.29	
MULTIFOIL INSULATION (Mo/Quartz)		5.94		7.16
SIDES	5.26		5.52	
ENDS	0.68		0.55	
SUPPORT STRUCTURE	----		1.09	
RTG HOUSING (Al)		8.45		8.17
SIDE WALL (0.090"/0.060")	7.01		6.47	
COVERS & BOLTS	0.98		0.81	
RESISTANCE THERMOMETER	0.30		0.30	
GAS MGMT. ASSEMBLY	0.16		0.16	
PRESSURE RELEASE DEVICE	----		0.43	
RADIATOR		2.78		3.00
FINS (8/8)	2.38		1.96	
AUXILIARY COOLANT MANIFOLDS	0.25		0.26	
EMISSIVITY COATING	0.15		0.15	
MISCELLANEOUS ELEMENTS	----		0.63	
TOTAL RTG MASS (kg)		58.67		56.08

The left column of Table 1 shows that the baseline RTG has a total mass of 58.7 kg. As shown, most (58%) of that mass is in the heat source rather than the converter, and most of that (77%) resides in the heat source modules. It is also noteworthy that the heat source canister, which enables operation of the RTG in the Martian atmosphere, has a mass of 3.8 kg.

The right half of Table 1 shows the corresponding mass breakdown for the existing Galileo RTGs. As seen, the baseline Rover RTG, with its non-optimized radiator fins, is 4.6% heavier than the Galileo RTG. A major part of that difference (3.77 kg) is due to the canister needed for Mars operations. The other subsystems have very similar masses in the two RTGs.

MASS OF HALF-LENGTH RTG

The preceding design assumed that the Rover's 500-watt power requirement would be met by two 250-watt RTGs. For ease of integration, it may prove preferable to employ four 125-watt RTGs, even though these would have a lower efficiency and lower specific power, because of increased end-section heat losses and masses. To assess that option, the reduction in efficiency and specific power must be quantified, to support the Rover design trade-off.

Table 2 presents a mass comparison between the two options. For ease of comparison, the table presents masses not for the single RTGs but for the full set of RTGs required to produce 500 watts. The basic design of the half-length RTG is essentially the same as that of the full-length RTG. The only change, besides the 50% reduction in the number of heat source modules and number of unicouple rings, is a decrease in the wall thickness of the RTG housing from 0.090" to 0.060", and a reduction from three parallel Belleville springs to one. These changes from the full-length unit are made possible because that the half-length housing is subjected to lower bending moments under traverse loads, and the half-length heat source stack can be held together with only about one fourth the axial preload.

Tale 2 shows that the use of four short RTGs instead of two long ones leads to a doubling of the mass of the RTG end sections, including the bellows, graphite pressure plates, load studs, zirconia insulators, other preload hardware, multifoil end insulation, housing ends and covers, and of the mass of the resistance thermometer, gas management assembly, and auxiliary coolant manifolds. In addition, there is also a significant increase in the mass of the canister end caps and load spreaders and of the radiator fin extensions. The total mass addition for the short-RTG option add up to 12.3 kg. But these additions are offset by reductions in the mass of the Belleville springs and of the RTG housing side wall totaling 5.1 kg. Thus, the use of four short RTGs leads to a net mass increase of only 7.2 kg or 6.2%.

MASS OF MULTICOUPLE RTG

Tables 1 and 2 presented the mass summaries of the unicouple RTGs depicted in Figures 10 and 11 of the preceding paper [1]. Table 3 presents the mass summary of the multicouple RTG depicted in Figures 13 and 14, and compares it to that of the baseline unicouple RTG.

The two RTGs have the same EOM power goal, 250 watts per RTG. The unicouples and

Table 2. Mass of "250-W" RTGs Versus "125-W" RTGs

RTG MASS BREAKDOWN (kg)	TWO 250-W RTGS	FOUR 125-W RTGS	Δ
HEAT SOURCE			
GPHS MODULES (18 9)			
FUEL (PuO2)	21 46	21 46	0
CAPSULES (Ir)	8 42	8 42	0
GRAPHITICS	22 22	22 22	0
H.S CANISTER (Mo)			
SIDE WALLS	4 42	4 42	0
BELLOWS	0 22	0 44	0 22
END CAPS AND LOAD SPREADERS	2 90	4 64	1 74
H S STRUCTURAL SUPPORTS			
GRAPHITE PRESSURE PLATES	1 04	2 08	1 04
LOAD STUDS+ZIRCONIA	0 54	1 08	0 54
BELLEVILLE SPRINGS (Ti)	4 62	2 20	-2 42
OTHER PRELOAD HARDWARE	1 68	3 36	1 68
CONVERTER			
ELECTRICAL CIRCUITS			
TE ELEMENTS (576/288)	10 86	10 86	0
TE FASTENERS AND SEALS	2 18	2 40	0 22
ALUMINA INSULATORS	1 76	1 76	0 00
ELECTR CONNECTORS +TERMINALS	0 68	0 80	0 12
MULTIFOIL INSULATION (Mo/Quartz)			
SIDES	10 52	10 52	0
ENDS	1 36	2 72	1 36
RTG HOUSING (Al)			
SIDE WALL (.090"/.060")	13 08	10 44	-2 64
END SECTION	0 94	1 88	0 94
COVERS	1 96	3 92	1 96
RESISTANCE THERMOMETER	0 60	1 20	0 60
GAS MGMT ASSEMBLY	0 32	0 64	0 32
RADIATOR			
FINS (8/8)	4 76	5 72	1
AUXILIARY COOLANT MANIFOLDS	0 50	1 00	0 50
EMISSIVITY COATING	0 30	0 40	0 10
TOTAL MASS(kg)	117 34	124 58	7 24

Table 3. Mass of Unicouple RTG Versus Multicouple RTG

RTG MASS BREAKDOWN (kg)	UNICOUPLE RTG BASELINE DESIGN	MULTICOUPLE RTG
HEAT SOURCE		
GPHS MODULES (18 16)		
FUEL (PuO2)	10 73	9 54
CAPSULES (Ir)	4 21	3 74
GRAPHITICS	11 11	9 88
H.S. CANISTER (Mo)		
SIDE WALLS	2 21	1 97
BELLOWS	0 11	0 10
END CAPS AND LOAD SPREADERS	1 45	1 45
H.S STRUCTURAL SUPPORTS		
GRAPHITE PRESSURE PLATES	0 52	0 52
LOAD STUDS+ZIRCONIA	0 27	0 27
BELLEVILLE SPRINGS (Ti)	2 31	1 27
OTHER PRELOAD HARDWARE	0 84	0 53
CONVERTER		
ELECTRICAL CIRCUITS		
TE ELEMENTS (576/128)	5 43	2 09
TE FASTENERS AND SEALS	1 09	0 49
ALUMINA INSULATORS	0 88	----
ELECTR CONNECTORS +TERMINALS	0 34	0 26
MULTIFOIL INSULATION (Mo/Quartz)		
SIDES	5 26	3 44
ENDS	0 68	0 59
RTG HOUSING (Al)		
SIDE WALL (.090"/.080")	6 54	5 20
END SECTION	0 47	0 38
COVERS	0 98	0 74
RESISTANCE THERMOMETER	0 30	0 30
GAS MGMT ASSEMBLY	0 16	0 16
RADIATOR		
FINS (8/4)	2 38	1 93
AUXILIARY COOLANT MANIFOLDS	0 25	0 25
EMISSIVITY COATING	0 15	0 15
TOTAL MASS(kg)	58 67	45 25

multicouples both use SiGe legs, but the N-legs of the multicouples that were tested contained a GaP additive, which raises the couples' BOM figure of merit (Z) from 0.00058 K^{-1} to 0.00072 K^{-1}. This increases the BOM material efficiency from 7.86% to 8.57%. As a result, the multicouple RTG can achieve its 250-watt output goal with a lower thermal input power. Therefore, the multicouple RTG design is based on 16 rather than 18 heat source modules, as indicated in the table.

As shown in Table 3, the total mass of the multicouple RTG is 23% lower than that of the baseline RTG (45.3 kg versus 58.7 kg). One of the primary causes of that mass reduction is the smaller number of heat source modules and the resultant shorter RTG length. The shorter length not only has a direct effect on the mass of the RTG housing and the heat source canister, but also results in additional mass savings: the housing wall thickness can be reduced, because the bending moments on the cantilevered structure are lower; and the mass of the Belleville springs is reduced because the axial preload to hold the heat source stack together is lowered.

In addition to the above mass savings, which result from the higher thermoelectric material efficiency, there are also significant savings deriving from the thermal insulation used in the multicouple RTG. Elimination of the quartz cloth spacers between the 60 layers of Mo foil results in direct mass savings and in significant indirect savings. The latter occur because the much thinner insulation package and shorter TE legs reduce the RTG housing diameter from 9.1" to 7.5". The table reflects the net result of all these mass changes.

Parenthetically, it should be noted that unicouples with GaP-doped N-legs may also be possible. But these have not yet been built and tested, and their development would not be a trivial material substitution because the two types of TE elements employ substantially different hot-junction bonding methods.

RTG THERMAL ENVIRONMENT

The various RTG designs were analyzed for the following four combinations of thermal power and cooling:

1) Beginning-of-Mission (BOM), assumed to be 3 years after fueling, on a hot ($300^{o}K$) summer day on Mars, to determine the RTG's maximum hot-junction and clad operating temperatures to confirm that they did not exceed established limits.

2) End-of-Mission (EOM), assumed to be 7 years after fueling, on a hot summer day on Mars, to compare the EOM power output with the design goal.

3) EOM on a cold ($140^{o}K$) winter night on Mars, to determine the effect of a cold environment on EOM power.

4) BOM with the RTG contained within the Rover's aeroshell and with its fins cooled by an auxiliary coolant loop, to determine the power output and RTG temperatures during transit to Mars. (The auxiliary cooling tubes were tentatively assumed to have a wall temperature of $100^{o}C$).

All the design analyses completed to date were based on the unrealistic assumption that each RTG has an unobstructed view of space and of the Martian ground. In addition, we plan to analyze the case of four 125-RTGs mounted in parallel on top of the Rover, at its four corners, to assess the effect of mutual blockage of their radiators. This is a concept currently favored by some Rover designers at JPL.

THERMAL AND ELECTRICAL ANALYSIS

The analysis described in this section consists of three parts (thermal, thermoelectric, and electrical), which must be performed simultaneously and interactively. The analysis uses specialized computer codes generated by Fairchild to compute the heat flows, temperatures, and electrical parameters of each layer of thermoelectric elements. Inputs include the RTG design, the thermal input power (BOM/EOM), the cooling mode (water/radiation, Mars environment), the TE materials and performance, and the desired electrical output voltage.

The thermal analysis employs a 425-node SINDA model of the axisymmetric RTG to compute the axial variation of the temperatures of the various RTG components. That axial variation is appreciable, because of unavoidable end losses through the structural supports at the top and bottom of the heat source stack. Each heat source module and thermoelectric element layer is discretely represented in the SINDA model.

The computed heat flow through the various TE elements includes the effects of Peltier cooling; ohmic heating in legs, electrodes, and leads; heat converted to electricity (i.e., the TE legs effectively act as heat sinks); and heat losses through multifoil, glass, and quartz yarn wrap.

The thermoelectric analysis includes the effects of measured contact resistances and ohmic losses in legs, electrodes, and leads; experimentally determined effects of long-term material degradation of SiGe; and optimized n/p leg area ratios. Other constraints are that all TE elements in series must have the same current, and all in parallel must have the same voltage.

The analysis uses temperature-dependent values of the Seebeck coefficient, electrical resistivity, and thermal conductivity for the SiGe N and P legs, with a temperature-averaged figure of merit (Z) of 0.000583 K^{-1} at BOM and 0.000548 K^{-1} at EOM for the baseline SiGe unicouple. The thermal and electrical results are used to compute the material efficiency, couple efficiency, and converter efficiency of each layer of TE elements, and the overall RTG system efficiency.

The thermal analysis of the initial design assumed an RTG housing wall thickness of 0.090"

and eight radiator fins of a trapezoidal cross-section, with a fin root thickness of 0.060", a fin tip thickness of 0.015", and a root-to-tip fin height of 3.0". The fins have an axial length of 42.7". Thus, they extend 2.5" beyond each end of the active thermoelectric zone. These dimensions were based on the results of a preliminary structural analyses described in the next paper at this conference [2].

TEMPERATURE DISTRIBUTION OF BASELINE RTG

Figure 1 shows the BOM temperature distribution (in ^{o}C) of the radiation-cooled baseline RTG for a $300^{o}K$ sink temperature. It shows the temperatures of the RTG end regions, and the temperatures at the center of the RTG. The temperatures shown are for an RTG with unicouples of standard dimensions, except that the cross-sectional areas of their SiGe legs have been reduced by 9% from the corresponding values in the Galileo RTG. This was done in order to take full advantage of the unicouples' maximum temperature capability.

Figure 1. BOM Temperature Distribution (°C) in Baseline RTG

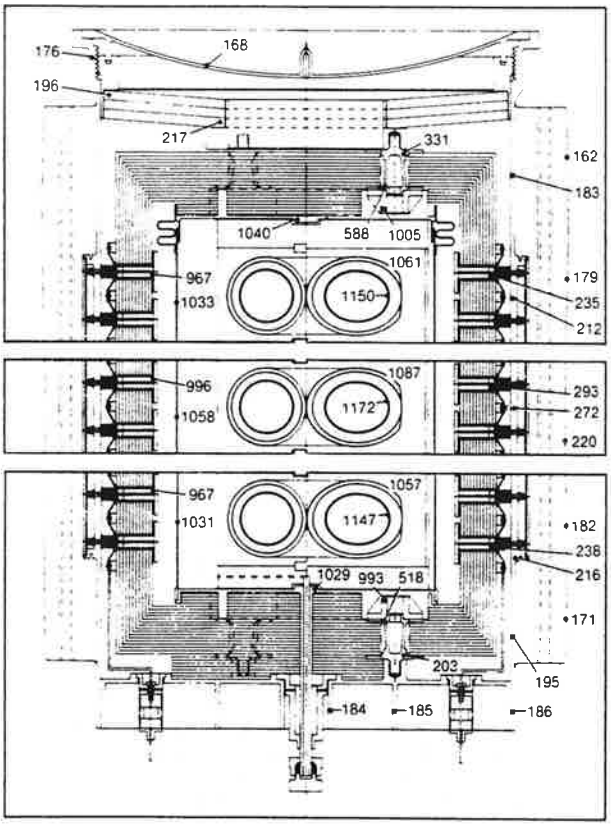

The figure shows the maximum temperatures of the iridium ($1172^{o}C$), the graphite heat source surface ($1087^{o}C$), the molybdenum canister ($1058^{o}C$), the SiGe hot junction ($996^{o}C$) and cold junction ($293^{o}C$). Of particular interest are the maximum temperatures of the zirconia insulators ($1005^{o}C$), the Inconel support studs ($588^{o}C$), the titanium springs ($217^{o}C$), and the aluminum housing ($272^{o}C$), since their mechanical properties and creep characteristics are strong functions of temperature.

To illustrate the approach used in the thermal, thermoelectric, and electrical analyses of the various RTG designs, the BOM results for the baseline RTG radiating to a $300^{o}K$ sink are presented in detail in Figures 2, 3, and 4. (Similar detailed results were generated for each design option and each environment investigated.)

AXIAL VARIATION OF HEAT FLOW RATES

The BOM temperatures shown in Figure 1 result in the axial variation of heat flow rates to and from each ring of thermoelectric unicouples and their associated converter sections shown in Figure 2.

Figure 2. Axial Variation of Heat Flow Rates

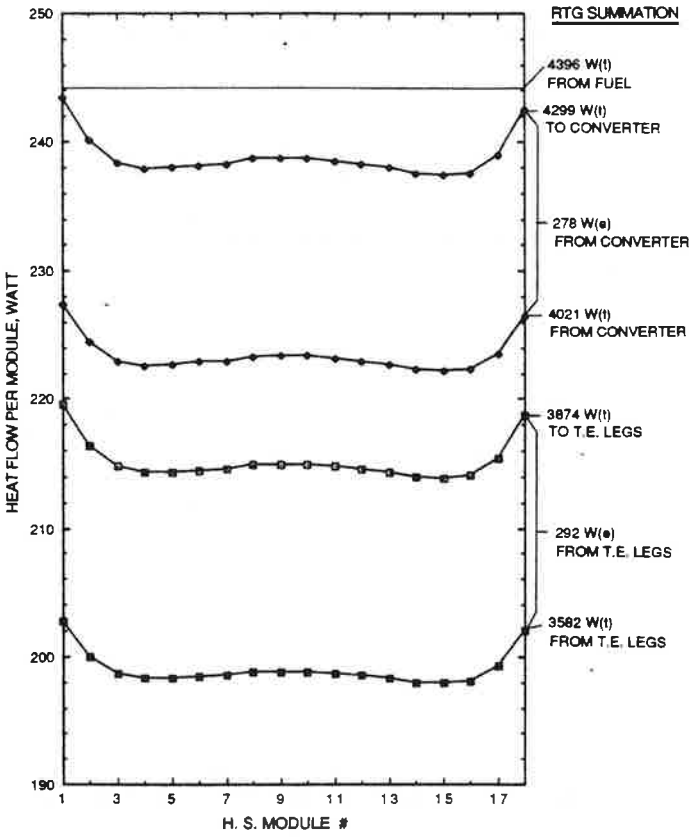

The numbers at the right edge of the figure show the summed heat flows for the whole RTG. As can be seen, this RTG design has a thermal efficiency of 3874/4396 = 88%. The 97-watt difference between the 4396 watts generated by the fuel and the 4299 watts flowing to the converter represents the axial heat loss from the ends of the heat source stack; and the 425-watt difference between the heat flow to the converter and the 3874 watts flowing to the TE legs represents the heat losses through the thermal insulation and quartz yarn wrap surrounding the TE elements.

The 292-watt difference between the heat flows to and from the TE legs (curves 4 and 5) represents the gross electrical power output; and the 278-watt difference between the heat flows to and from the converter (curves 2 and 3) represents the net electrical power output, after lead losses.

AXIAL TEMPERATURE PROFILES

Figure 3 depicts the axial temperature variations in the RTG. The heat losses from the end of the heat source stack result in the depicted temperature profiles of the fuel capsule clads, the modules' aeroshell surfaces, the canister, and the unicouple hot junctions. The figure also shows the axial temperature variations of the cold junctions, the fin root, and the fin tip.

Figure 3. Axial Temperature Profiles

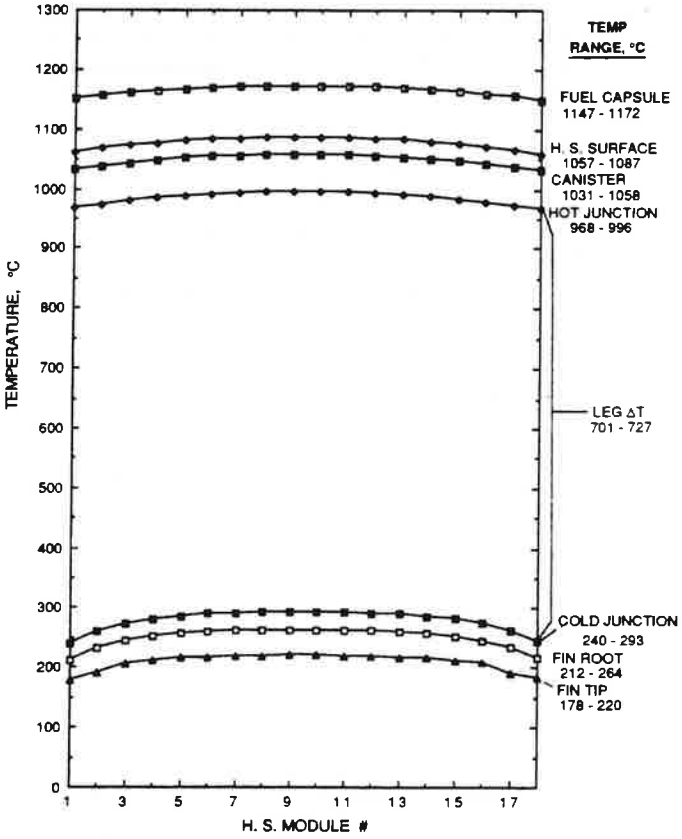

The figure shows six temperature drops between the various curves. The first (~85°C) represents the drops inside the heat source modules, across the graphitics and helium gaps. The second (~29°C) is the drop across the helium gap to the canister, and the third (~62°C) is across the vacuum gaps and through the TE heat collectors. The fourth (703 to 728°C) is the temperature drop across the SiGe TE legs. As can be seen, this is the largest of the drops. It is the only one that makes a useful contribution in actually generating electrical power. All the other temperature drops represent thermodynamic losses. The fifth drop (~29°C) represents the thermal resistance of the unicouple's cold-end and the loss for circumferential heat transport through the aluminum housing to the nearest fin; and the sixth drop (44°C) is that due to radial heat flow through the fin itself.

The depicted variation of the hot-junction temperatures would result in a significant performance loss, were it not balanced by a similar convex profile of the cold-junction temperatures. This was achieved by extending the radiator fins beyond the active length of the RTG, as mentioned earlier. In fact, the temperature drop-off of the cold junctions near the RTG ends is greater than that of the hot junctions. This explains why the unicouples' heat flow rates, power outputs, and efficiencies are actually higher at the ends of the RTG than at the center, as shown in Figures 2 and 4.

AXIAL VOLTAGE AND EFFICIENCY PROFILES

The temperature variations shown in Figure 3 result in the unicouple voltage and efficiency profiles displayed in Figure 4. The averaged values for the RTG are shown at the right edge of the figure. The 0.010-volt difference between the gross and net couple voltages represents the electrical losses in the leads.

Figure 4. Axial Voltage and Efficiency Profiles

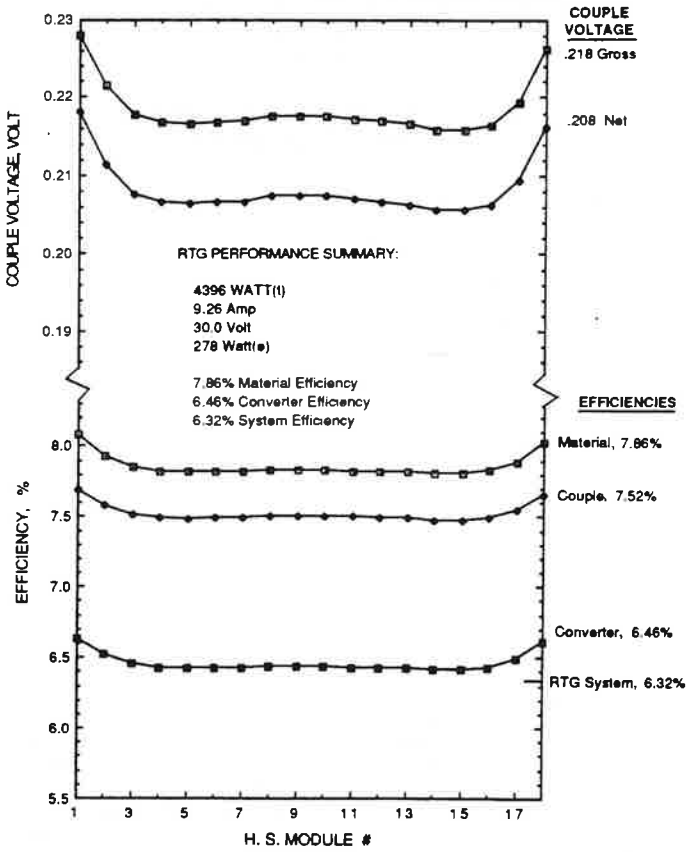

The difference between the 7.86% material efficiency and the 7.52% couple efficiency is the effect of ohmic losses in the electrodes. The difference between the couple efficiency and the 6.46% converter efficiency shown in the figure reflects the electrical losses in the leads and the thermal losses through the multifoil side

insulation and the quartz yarn wrap. As seen, the axial variation of the efficiencies is quite small. In fact, the couples near the ends have a higher efficiency because of their lower cold-junction temperatures, which result from axially extending the radiator fins beyond the thermoelectric region. The 0.55-percentage-point difference between the overall converter efficiency and the 6.32% system efficiency reflects the heat losses through the RTG ends.

Figure 4 shows that there are substantial differences between the BOM material efficiency, couple efficiency, converter efficiency, and system efficiency. This highlights the importance of specificity in reporting RTG efficiencies.

EFFECT OF COOLING MODE ON RTG PERFORMANCE

Table 4 illustrates the effect of the cooling mode on the BOM temperature distribution, efficiencies, and output of the baseline RTG. The left column shows the results for the water-cooled RTG, representative of the launch and orbital transit conditions; the middle column present the corresponding results for the radiation-cooled RTG, representative of operations on a Martian summer day (300°K); and the right column shows similar results for a Martian winter night (140°K).

Table 4. Effect of Cooling Mode on BOM Performance of Baseline RTG

Cooling Mode	Convective	Radiative	
Auxiliary Coolant Wall Temp., °C	100	—	—
Radiator Sink Temperature, °K	300	300	140
Maximum Temperature, °C:			
Fuel Clad	1089	1172	1166.
H.S. Surface	992	1087	1080
Canister	957	1058	1051
TE Hot Junction	888	996	988
TE Cold Junction	155	293	284
Fin Root	117	264	254
Fin Tip	94	220	210
Efficiency, %:			
Material	7.97	7.86	7.88
Couple	7.51	7.52	7.53
Converter	6.50	6.46	6.48
System	6.37	6.32	6.32
RTG Output:			
Current, amp	9.26	9.26	9.26
Voltage	30.2	30.0	30.1
Power	280	278	278
Specific Power, watt/kg	4.77	4.74	4.74

The left and middle fin root temperatures are used to compute the differential thermal expansion of the aluminum housing, which dictates the required Belleville spring travel of 0.099". This thermal expansion difference results in a relaxation of the axial spring load. Consequently, the lateral G-loads that the heat source stack can tolerate are 40% lower on Mars than during launch.

Comparison of the three sets of efficiencies and RTG outputs show almost identical results for the three cases. This is because, for a fixed design, changes in the cold-junction temperatures cause similar changes in the hot-junction temperatures; and because the temperature-integrated thermoelectric properties of SiGe are not very sensitive to cold-junction temperature. As a result, the power output of the RTG is quite insensitive to thermal environment, so that the RTG can produce essentially the same power during launch and during transit to Mars as that generated on Mars in either summer or winter. We therefore conclude that the RTG can deliver full operating power during the water-cooled cruise to Mars; and that the power output of the radiatively cooled RTG is essentially independent of the Martian temperature.

EFFECT OF LIFETIME ON RTG PERFORMANCE

Table 5 illustrates the change from BOM (3 years after fuel encapsulation) to EOM (7 years after fuel encapsulation) on the output of the radiation-cooled baseline RTG with a 300°K sink temperature. The left column displays the BOM temperatures and output voltage, current, power, and efficiencies of the RTG, and the right half shows the corresponding EOM values.

Table 5. Effect of Mission Time on Performance of Baseline RTG

Mission Time	BOM	EOM
Years After Fuel Encapsulation	3	7
Years of Full-Temperature TE Operation	1	5
Thermal Power, watts	4396	4261
Maximum Temperature, °C:		
Fuel Clad	1172	1152
H.S. Surface	1087	1065
Canister	1058	1037
TE Hot Junction	996	975
TE Cold Junction	293	289
Fin Root	264	260
Fin Tip	220	218
Efficiency, %:		
Material	7.86	7.41
Couple	7.52	7.12
Converter	6.46	6.13
System	6.32	6.01
RTG Output:		
Current, amp	9.26	8.52
Voltage	30.0	30.0
Power, watt	278	256
Specific Power, watt/kg	4.74	4.37

The biggest cause of power output change during that period is the decay of the radioisotope fuel, which has a half-life of approximately 89 years. As a result, the original 4500-watt thermal power of the 18-module heat source drops to 4396 watts at BOM and to 4261 watts at EOM. As shown in Table 5, this lowers the maximum clad temperature from 1172°C to 1152°C, drops the maximum hot-junction temperature from 996° to 975°C, and reduces the maximum temperature drop in the SiGe legs from 703°C to 686°C.

This temperature drop reduction lowers the conversion efficiency. The reduced thermal power and reduced efficiency combine to cause a greater-than-proportional reduction in power output. This would be true even if there were no concurrent degradation in thermoelectric

properties of the SiGe. But there is a well-characterized material degradation, primarily because of dopant precipitation. As a result, the system efficiency actually drops from 6.32% to 6.01% and the power output drops from 278 watts to 256 watts, as shown in the table. We therefore conclude that the combined effect of fuel decay and thermoelectric degradation is to reduce the power output by ~8%.

Table 5 shows that the power output of the baseline RTG exceeds the goal of 250 watts EOM, without exceeding the 1000°C hot-junction temperature limit or the 1330°C clad limit.

EFFECT OF RTG LENGTH ON PERFORMANCE

The masses of the two "250-watt" RTGs were compared with those of four "125-watt" RTGs in Table 3. The temperatures, efficiencies, and outputs for the two options are compared in Table 6, both for BOM and EOM.

Table 6. Effect of RTG Length on Performance

Number of HS Modules per RTG	18		9	
RTG Length, inches	45.9		26.3	
Nominal EOM Power per RTG, watts	250		125	
Number of RTGs on Rover	2		4	
Mission Time	BOM	EOM	BOM	EOM
Thermal Power per RTG, watt	4396	4261	2198	2131
Maximum Temperature, °C				
Fuel Clad	1172	1152	1172	1153
H.S. Surface	1087	1065	1086	1067
Canister	1058	1037	1059	1039
TE Hot Junction	996	975	998	980
TE Cold Junction	293	289	275	271
Fin Root	264	260	247	243
Fin Tip	220	218	206	203
Efficiency, %				
Material	7.86	7.41	8.07	7.58
Couple	7.52	7.12	7.72	7.29
Converter	6.46	6.13	6.61	6.26
System	6.32	6.01	6.32	5.96
Output of Set of RTGs				
Current, amp	18.5	17.0	18.3	18.3
Voltage	30.0	30.0	30.2	30.2
Power, watt	556	512	556	508
Mass of Set of RTGs, kg	117.3	117.3	124.6	124.6
Specific Power, watt/kg	4.74	4.37	4.46	4.08

The table shows that the short RTGs also meet their design goal (125 watt EOM per RTG) without exceeding the 1000°C hot-junction temperature limit. It shows that the system efficiency of the short RTG is almost as high as that of the long RTG.

This was not expected, because the four short RTGs have twice as many end sections and obviously have greater heat losses from the ends of their heat source stacks. Evidently, these losses are compensated by their higher converter efficiencies, as shown in the table. Their higher converter efficiency is due to their lower cold-junction temperature (271°C versus 289°C) which results from the greater effectiveness of the axial radiator extensions in the short RTGs. It should be noted, however, that the radiator fin design has not yet been optimized for either the long or the short RTGs.

Table 6 shows that the specific power of the short RTGs is 9% lower than that of the long ones. This is primarily due to their higher mass rather than lower system efficiency. The difference in specific power between the two options is small enough to make the short RTG option a viable alternative to the baseline design, if the shorter units are indeed easier to integrate with the Rover (e.g., because the shorter RTGs are less prone to block the Rover's sensors and/or antennas). But this conclusion will have to be re-examined after the effect of mutual radiator blockage of multiple RTGs is taken into account.

An additional advantage of the short RTGs is that if one of the four should experience catastrophic failure before the end of the mission, the other three would still supply 75% of the Rover's design power, permitting continued Mars operations on a limited scale.

MULTICOUPLE RTG PERFORMANCE

The preceding paper [1] described basic designs for RTGs employing standard unicouples (UC) and standard multicouples (MC). The multicouple RTG design shown in Figures 13 and 14, with demonstrated MC performance parameters, was subjected to detailed thermal, thermoelectric, and electrical analyses, identical to those performed for the baseline (unicouple) RTG.

The results of those analyses for the two RTGs are summarized in Table 7, which compares their temperatures, efficiencies, output powers, and specific powers. Both cases are for

Table 7. Performance of Multicouple RTG Versus Unicouple RTG

Thermoelectric Elements	Unicouples		Multicouples	
Number of Elements	576		128	
Number of H.S. Modules	18		16	
RTG Length, inches	45.9		41.6	
RTG Housing Diameter, inches	9.1		7.5	
N-Leg Material	SiGe		SiGe/GaP	
Couple Figure of Merit, K^{-1}	0.00058		0.00072	
Number of Fins	8		4	
Fin Root Thickness, inch	0.060		0.100	
Fin Length, inches	3.0		5.5	
Mission Time	BOM	EOM	BOM	EOM
Thermal Power per RTG, watt	4396	4261	3907	3787
Maximum Temperature, °C:				
Fuel Clad	1172	1152	1171	1154
H.S. Surface	1087	1065	1085	1068
Canister	1058	1037	1057	1040
TE Hot Junction	996	975	1009	991
TE Cold Junction	293	289	315	309
Fin Root	264	260	259	255
Fin Tip	220	218	184	182
Efficiency, %:				
Material	7.86	7.41	8.57	8.14
Couple	7.52	7.12	8.01	7.60
Converter	6.46	6.13	7.05	6.68
System	6.32	6.01	6.76	6.42
RTG Output:				
Current, amp	9.3	8.5	9.0	8.3
Voltage	30.0	30.0	29.5	29.5
Power, watt	278	256	264	243
RTG Mass, kg	58.6	58.6	45.3	45.3
Specific Power, watt/kg	4.74	4.37	5.83	5.37

S-139.82 06-89C

radiation cooling with a 300°K heat sink. The unicouples employed SiGe n- and p-legs, with a BOM figure of merit (Z) of 0.00058. In the case of the multicouples, the n-legs contain a GaP additive, which raises the BOM Z to 0.00072. Both cases employed measured values of contact resistances for their respective TE elements. Because of its higher Z and anticipated higher efficiency, the multicouple RTG used 16 instead of 18 heat source modules.

Table 7 shows very similar temperatures for the RTGs, with two exceptions. The first is that the temperature drop from the cold junction to the fin root is much higher (56°C) in the multicouple-RTG than in the unicouple-RTG (29°C). This is due to the fact that each multicouple rejects much more heat than a unicouple, and that this heat has to flow through a greater distance to reach the nearest fins, since the MC-RTG has only four fins instead of eight.

The second difference between the two RTGs is that the root-to-tip temperature drop in the fins is appreciable greater (75°C) in the MC RTG than in the UC unit (44°C). This is due to the fins' greater length, which is necessitated by the smaller number of fins.

In spite of these increased temperature drops, the MC RTG shows virtually the same system efficiency the UC RTG. This is due to the use of the GaP additive in the n-legs, which raises the figure of merit from 0.00058 K^{-1} to 0.00072 K^{-1}, and the BOM material efficiency from 7.86% to 8.57%. As shown in Table 7, the MC RTG with 16 heat source modules produces 5% less power than the UC RTG with 18 heat source modules. In fact, it falls a little below its 250-watt EOM goal.

The last two lines of Table 7 compare the masses (from Table 3) and the specific powers of the two RTGs. As can be seen, the specific power of the MC RTG is 23% higher than that of the UC RTG. This benefit must be weighed against their lower technological maturity and higher programmatic risk.

EFFECT OF THERMOELECTRIC MATERIAL PROPERTIES

Materials Studied: The results thus far were all based on demonstrated thermoelectric properties of the SiGe unicouples and the SiGe/GaP multicouples. The present section examines the effect which improvements of those properties would have on the RTG designs and on their mass and performance. RTGs based on five different material models were analyzed:

1. The first is a JPL model for SiGe, with 78% Si in the hotter 85% of the TE legs and 63% Si in the cooler 15% of the leg. This is the same material model used in our baseline design analysis, and is representative of the unicouples used in the Galileo RTGs. At BOM, it yields a figure of merit of 0.000584 K^{-1} over a 1000°C-to-300°C temperature range.

2. The second material model employed is designated ITM-197. The material's thermoelectric properties have been confirmed by measurements at independent laboratories, but it has not yet been built into a couple. Its BOM figure of merit is 0.000768 K^{-1}.

3. The third material model, designated GE Hybrid, represents the materials used in the multicouples built and tested to date. It was used as the basis for our multicouple design. Its BOM figure of merit (Z) is 0.000782 K^{-1}. It has not yet been built into unicouples. Doing so would require development of new bonding techniques.

4. The fourth material model, designated SP-100, represents the thermoelectric performance parameters assumed for the SP-100 reactor system reference design. It assumes a GaP-doped n-leg (Z=0.00111) and a SiGe p-leg with an as-yet undefined additive (Z=0.00069), yielding a couple Z of 0.00085 K^{-1}. This performance level has not yet been achieved.

5. The fifth material model is designated "dream". Its composition and development pathway are not known to the authors. It was included at JPL's request, to quantify what effect a figure of merit of 0.00140 K^{-1} would have on RTG performance, if such a material could be successfully developed.

Assumptions: The five RTG designs were based on the same basic arrangement, i.e., the baseline design employing 16 unicouples (of 0.8" leg length) per horizontal ring, connected four in parallel. However, the number of heat source modules, the number of unicouples, and the cross-sectional areas of the unicouple legs were varied to meet (or come close to) the RTG voltage and power goals. The voltage goal used was 30 volts after lead losses; and the power goal was 250 w EOM or 280 w BOM after lead losses. Each of the five material models employed temperature-dependent resistivities, conductivities, and Seebeck coefficients for the n- and p-legs.

The primary emphasis in the design studies and analyses was to determine the relative RTG performance for the five options, rather than their absolute values. For this reason, and in the interest of expediency, a number of approximating assumptions were made:

The axial variations of the heat flow rates, temperatures, and couple outputs were ignored. All couples were assumed to operate at the same hot-junction temperature (1000°C) and cold-junction temperature (300°C) employed in previous RTG tests. In addition, the fraction of the generated heat that flows to the thermoelectric couples was assumed to be 88%, based on the results of the more detailed and exact analysis of the baseline RTG design.

Based on the same analysis, the effect of the electrode resistances and the electrical contact resistance were accounted for by increasing the materials' resistivities by 10%; and the effect of electrical lead losses was accounted for by subtracting 6% from each couple's output voltage.

Finally, the number of thermoelectric rings per heat source module had been arbitrarily fixed at 2.0 in the baseline design (for consistency with the Galileo RTG), but was varied in each of the five comparison designs so as to maximize the conversion efficiency.

Because of these differences in analytical approach, the results of the material comparison analysis are not an exact match to those of the baseline RTG analysis. But the comparison analysis is internally consistent, and its results are a valid comparison of the relative RTG performance for the five TE materials.

Thermoelectric Analysis: The critical material properties of a thermoelectric couple are the temperature-dependent Seebeck coefficient S', thermal conductivity k', and electrical resistivity ρ' of its n- and p-legs. The first step in the analysis is to use these to compute the temperature-averaged values:

$$S = \int_{T_c}^{T_h} (S_n' + S_p')\, dT / \Delta T \quad , \tag{1}$$

$$k_n = \int_{T_c}^{T_h} k_n'\, dT / \Delta T \quad , \tag{2}$$

$$k_p = \int_{T_c}^{T_h} k_p'\, dT / \Delta T \quad , \tag{3}$$

$$\rho_n = \int_{T_c}^{T_h} \beta\, k_n' \rho_n'\, dT / k_n\, \Delta T \quad , \text{and} \tag{4}$$

$$\rho_p = \int_{T_c}^{T_h} \beta\, k_p' \rho_p'\, dT / k_p\, \Delta T \quad , \tag{5}$$

where T_h and T_c are the assumed hot- and cold-junction temperatures, ΔT is the difference between them, and the factor β accounts for the resistances of the contacts and the electrodes. Based on the detailed analysis of the baseline RTG, a value of 1.10 was used for β.

A thermoelectric couple with n- and p-legs of length L and combined cross-sectional area A has a thermal conductance

$$K = [k_n \alpha + k_p(1-\alpha)]\,(A/L) \tag{6}$$

and an electrical resistance

$$R = [\rho_n/\alpha + \rho_p/(1-\alpha)]\,(L/A) \quad , \tag{7}$$

where α is the area fraction of the n-leg and $1-\alpha$ is the area fraction of the p-leg. If the couple operates at a current I, the heat input rate Q_h at its hot junction is given by

$$Q_h = K\Delta T + IST_h - I^2R/2 \quad , \tag{8}$$

where the first term represents the zero-current heat conduction, the second term is the Peltier cooling rate of the hot junction, and the third term represents one half of the ohmic heat dissipation rate in the couple. Similarly, the heat rejection rate Q_c at the couple's cold junction is given by

$$Q_c = K\Delta T + IST_c + I^2R/2 \quad , \tag{9}$$

Subtracting Eq. (9) from (8), we obtain

$$Q_h - Q_c = IS\Delta T - I^2R \quad . \tag{10}$$

The couple voltage V is given by the difference between the open-circuit voltage $S\Delta T$ and the internal voltage drop IR,

$$V = S\Delta T - IR \quad . \tag{11}$$

Eliminating $S\Delta T$ between Eqs. (10) and (11), we obtain

$$Q_h - Q_c = IV \quad , \tag{12}$$

which is consistent with the energy balance for the couple. The couples conversion efficiency η is given by

$$\eta = \frac{IV}{Q_h} = \frac{IV}{K\Delta T + IST_h - I^2R/2} \quad . \tag{13}$$

Solving Eq. (11) for I and inserting the results into (13), we obtain

$$\eta = \frac{V(S\Delta T - V)}{KR\Delta T + ST_h(S\Delta T - V) - (S\Delta T - V)^2/2} \quad , \tag{14}$$

which is the general solution for the efficiency of a thermoelectric couple, before optimization of its leg area fraction α and its output voltage V. The optimum area fraction α is that value which minimizes the product KR in the denominator of Eq. (14). From Eqs. (6) and (7), that product is given by

$$KR = k_n\rho_n + k_p\rho_p + k_n\rho_p\left[\frac{\alpha}{1-\alpha}\right] + k_p\rho_n\left[\frac{1-\alpha}{\alpha}\right] \quad . \tag{15}$$

Note that for a given set of hot- and cold-junction temperatures the product KR, and therefore the efficiency η, are independent of the leg dimensions L and A. The product KR is minimized when

$$\alpha_{opt} = \left[1 + \sqrt{(k_n/k_p)\,(\rho_p/\rho_n)}\right]^{-1} \tag{16}$$

Inserting this into Eq. (15), we obtain the minimum value of the product KR,

$$(KR)_{min} = \left[\sqrt{k_n\rho_n} + \sqrt{k_p\rho_p}\right]^2 \quad . \tag{17}$$

Inserting Eq. (17) into (14) gives the efficiency η' of a couple with optimized leg area fraction,

$$\eta' = \frac{V(S\Delta T - V)}{\left[\sqrt{k_n\rho_n} + \sqrt{k_p\rho_p}\right]^2\Delta T + ST_h(S\Delta T - V) + (S\Delta T - V)^2/2} \quad , \tag{18}$$

The preceding expression is maximized by setting the couple output voltage equal to

$$V_{opt} = \frac{S\Delta T}{1 + \frac{1}{\sqrt{(1 + Z\bar{T})}}} \quad , \tag{19}$$

where Z is the thermoelectric materials' temperature-averaged figure of merit, defined by

$$Z \equiv \left[\frac{S}{\sqrt{k_n \rho_n} + \sqrt{k_p \rho_p}} \right]^2 \quad , \tag{20}$$

and T is the average temperature

$$\bar{T} = (T_h + T_c)/2 \quad . \tag{21}$$

Inserting Eq. (19) into (18) gives the maximum efficiency η'' of a couple with optimized leg fraction α and optimized output voltage V.

$$\eta'' = \frac{\left[\sqrt{(1 + Z\bar{T})} - 1\right] \eta_c}{\sqrt{(1 + Z\bar{T})} + 1 - \eta_c} \quad , \tag{22}$$

where η_c is the Carnot efficiency, which is a function of the absolute hot- and cold-junction temperatures:

$$\eta_c = 1 - T_c / T_h \quad . \tag{23}$$

Equations (19) and (22) show that the optimum couple voltage and maximum efficiency are functions of only the thermoelectric material properties and the operating temperatures. Figure 5 presents a semi-log plot of the voltage ratio $V_{opt}/S\Delta T$ as a function of $Z\bar{T}$, and Figure 6 presents a log-log plot of η'' versus $Z\bar{T}$ for various values of η_c. Figure 5 shows that the matched-load condition ($V=0.5\ S\Delta T$) does not yield the maximum efficiency. The greater the value of $Z\bar{T}$, the greater the deviation from matched load. Figure 6 shows that η'' is primarily a function of $Z\bar{T}$, and only weakly dependent on η_c.

Figure 5. Effect of Figure of Merit Z on Optimum Load Voltage V_{opt}

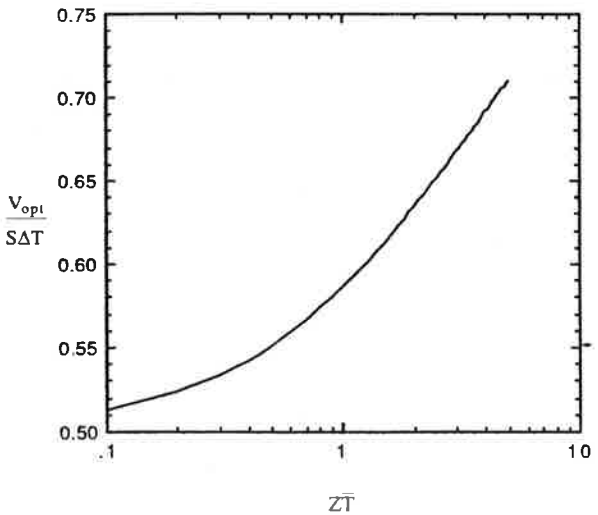

Figure 6. Effect of Figure of Merit Z and Carnot Efficiency η_c on Maximum Couple Efficiency η''

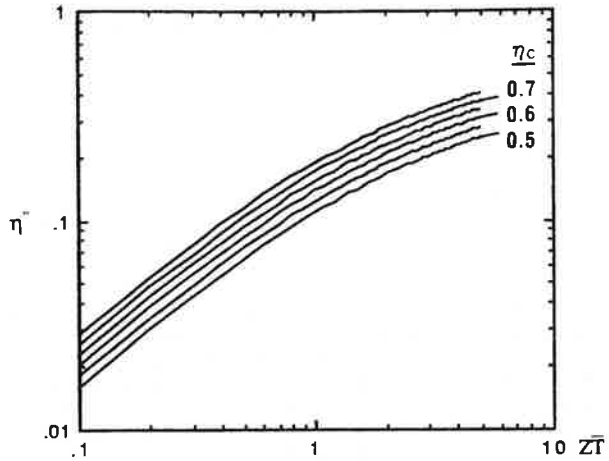

Consider now an RTG with N_m heat source modules, each having a heat generation rate Q_m. The RTG's power output P is given by

$$P = N_m Q_m \eta_t \eta'' (1 - \gamma) \quad , \tag{24}$$

where η_t is the RTG's thermal efficiency (i.e., the fraction of the generated heat delivered to the thermoelectric legs), η'' is the doubly-optimized couple efficiency given by Eq. (22), and γ is the fraction of the output voltage lost due to the electrical resistance of the inter-couple connectors and RTG terminals. The previous detailed analyses of the baseline RTG design yielded respective values of 0.88 and 0.06 for η_t and γ. To be consistent, those values were used throughout the material comparison studies.

Given a specified RTG power P, Eq. (24) can be solved for N_m, the number of heat source modules. But since N_m must be an integer, the RTG power goal can only be matched approximately. Alternatively, the power goal could be matched exactly, by deviating from the arbitrarily assumed cold-junction temperature T_c of 300°C (by adjusting the radiator fin dimensions).

The RTG has $N_p \times N_s$ thermoelectric couples, arranged in a network with N_p couples in parallel and N_s in series. For geometric reasons, N_p must of course be an integral divisor of the number of couples per ring. Given a specified RTG voltage, the number N_s of couples in series must satisfy the voltage balance

$$V_{RTG} = N_s V_{opt} (1 - \gamma) \quad , \tag{25}$$

where V_{opt} is the optimum couple voltage given by Eq. (19). Equation (25) can be solved for the integer value of N_s which comes closest to yielding the prescribed RTG voltage. Finally, we must solve for the couple's length-to-area ratio which satisfies the RTG's heat balance .

$$N_m Q_m \eta_t = N_p N_s Q_h \quad , \tag{26}$$

The heat input rate Q_h per couple is given by Eq. (3) in terms of its thermal conductance K, electrical resistance R, and current I. For the

optimum leg area fraction α_{opt} (Eq. 16) and couple voltage V_{opt} (Eq. 19), the equations for K, R, and I (Eqs. 6,7, and 11) can be reduced to

$$K = C_1(A/L) \ , \tag{27}$$

$$R = C_2(L/A) \ , \text{ and} \tag{28}$$

$$I = C_3(A/L) \ , \tag{29}$$

where $$C_1 \equiv k_n \left[\frac{1+\sqrt{(k_p/k_n)(\rho_p/\rho_n)}}{1+\sqrt{(k_n/k_p)(\rho_n/\rho_p)}}\right] \tag{30}$$

$$C_2 \equiv \rho_n \left[1+\sqrt{\frac{k_p\rho_p}{k_n\rho_n}}\right]\left[1+\sqrt{\frac{k_n\rho_n}{k_p\rho_p}}\right] \ , \text{ and} \tag{31}$$

and $$C_3 \equiv \frac{S\Delta T/C_2}{\sqrt{1+Z\bar{T}}+1} \ . \tag{32}$$

Inserting Eqs. (27), (28), and (29) into (8) and solving for L/A we obtain the expression

$$L/A = \left[C_1\Delta T + C_3 S T_h - C_2 C_3^2/2\right]/Q_h \tag{33}$$

for the required length-to-area ratio of the couples.

For each of the materials listed in the previous section, the preceding equations were solved for the RTG design parameters (N_m, N_p, N_s, α, and A) and for the resultant performance parameters (I, V, P, η^*) and the RTG's mass and specific power. The computed results are presented in the next section.

Results and Conclusions: Comparison of the five RTG designs showed, not surprisingly, that Materials 2, 3, and 4 yielded very similar results. Therefore, only the results for Options 1, 3, and 5 are presented below. Table 8 compares their performance, and Table 9 compares their mass breakdown.

Comparison of columns 1 and 2 of Table 8 shows that the addition of GaP in the SiGe n-leg produces very significant efficiency increases. For the same output power, these lead to substantial reductions in fuel loading and RTG mass.

Comparison of Columns 2 and 3 shows that the hypothetical and still undefined "dream" material would result in even greater efficiency increase, and correspondingly much larger reductions in fuel loading and RTG mass.

Multicouples employing SiGe/GaP n-legs have already been built and tested for 6000 hours. They exhibited stable performance under positive bias, but anomalous degradation under negative bias with respect to the RTG housing. Thus, they could be considered for use in RTGs in which all multicouples were maintained under positive bias. But if it were deemed too risky to fly a multicouple RTG until the negative-bias anomaly is more fully understood and resolved, Table 8 shows that the use of SiGe/GaP n-legs would still be quite advantageous for use in unicouple RTGs. Such unicouples have not yet been built, and would require significant new bond developments. But the programmatic risk of doing that seems reasonable and well justified by the potential payoff.

Table 8. Effect of Thermoelectric Figure of Merit on RTG Design and BOM Performance

Material:			
Material #	1	3	5
Designation	JPL 78/63	GE HYBRID	DREAM
BOM Figure Of Merit, K^{-1}	0.000584	0.000782	0.001387
RTG Design:			
Number of HS Modules	19	15	10
Thermal Power, watts	4640	3663	2442
RTG Height, inches	48.0	39.6	29.1
Number of Unicouple Rings	37	40	39
Unicouples per Ring	16	16	16
Number of Unicouples	592	640	624
Number in Parallel	4	4	4
Number in Series	148	160	156
Areas of TE Legs, cm^2	0.359	0.338	0.332
RTG Performance (BOM):			
Current, amp	9.30	9.13	9.08
Voltage	30.1	30.3	30.1
Power, watts	280	276	273
Couple Efficiency, %	7.26	9.08	13.48
System Efficiency, %	6.03	7.53	11.18
Estimated Mass, kg	61.6	50.9	37.7
Specific Power, w/kg	4.55	5.43	7.24

Table 9. Effect of Thermoelectric Material on Mass of Unicouple RTG

RTG MASS BREAKDOWN (kg)	JPL 78 63 Z=0 000584	GE HYBRID Z=0 000795	DREAM Z=0 001387
GPHS MODULES (19 15 10)			
FUEL (PuO_2)	11 12	8 94	5 06
CAPSULES (Ir)	4 44	3 51	2 74
GRAPHITICS	11 72	9 26	6 17
H S CANISTER (Mo)			
SIDE WALLS	2 23	1 84	1 23
BELLOWS	0 11	0 11	0 11
END CAPS AND LOAD SPREADERS	1 45	1 45	1 45
H S STRUCTURAL SUPPORTS			
GRAPHITE PRESSURE PLATES	0 52	0 52	0 52
LOAD STUDS+ZIRCONIA	0 27	0 27	0 27
BELLEVILLE SPRINGS (Ti)	2 64	1 22	0 35
OTHER PRELOAD HARDWARE	0 84	0 84	0 84
ELECTRICAL CIRCUITS			
TE ELEMENTS (592 640 624)	5 63	5 47	4 82
TE FASTENERS AND SEALS	1 12	1 21	1 18
ALUMINA INSULATORS	0 90	0 98	0 95
ELECTR CONNECTORS+TERMINALS	0 35	0 38	0 37
MULTIFOIL INSULATION (Mo Quartz)			
SIDES	5 53	4 43	3 62
ENDS	0 68	0 68	0 68
RTG HOUSING (Al)			
SIDE WALL (.090" .085" .060")	6 82	5 28	3 01
END SECTION	0 47	0 47	0 47
COVERS	0 98	0 98	0 98
RESISTANCE THERMOMETER	0 30	0 30	0 30
GAS MGMT ASSEMBLY	0 16	0 16	0 16
RADIATOR			
FINS (Al)	2 67	2 16	1 55
AUXILIARY COOLANT MANIFOLDS	0 25	0 25	0 25
EMISSIVITY COATING	0 15	0 15	0 15
TOTAL MASS(kg)	61 55	50 86	37 73

As for the dream material, the payoff would obviously be much greater. But they would require development of new material fabrication methods, bonding techniques, fabrication procedure, and extensive testing to demonstrate the couples' performance, reproducibility, compatibility with other RTG components at operating temperatures, and long-term performance stability. In the absence of any information about material compositions and development approach, the authors are unable to assess the ultimate success probability of such a development program. But, based on their extensive experience on numerous other RTG development programs, they are convinced that a program to develop a flight RTG employing this material would not come close to meeting the JPL-envisaged MRSR schedule described in Figure 2 of Reference [1].

REFERENCES

[1] A. Schock, V. Sankarankandath, and M. Shirbacheh, "Requirements and Designs of Mars Rover RTGs." 24th Intersociety Energy Conversion Engineering Conference, 6-11 August, 1989.

[2] A. Schock and T. Hamrick, "Structural Design and Analysis of Mars Rover RTGs." Ibid.

ACKNOWLEDGEMENT

The above work was supported by the U.S. Department of Energy's Office of Special Applications.

STRUCTURAL DESIGN AND ANALYSIS OF MARS ROVER RTGs

A. Schock, T. Hamrick

Fairchild Space Company, Germantown, MD

ABSTRACT

The paper presents the structural design and analysis of the Rover RTGs described earlier at this conference. Of particular importance are the axial preloads required to hold the stacked heat source modules together during Earth launch, Mars landing, and Mars roving. The paper describes the design and stress analysis of the heat source support structure, including the preload springs, and of the housing wall which supports the base-mounted cantilevered RTG. Although the Mars roving case produces lower G-loads than Earth launch, this case must also be analyzed and designed for, because the RTG cooling mode and RTG housing temperatures change after Mars landing, and the spring length and spring force will change correspondingly. The structural analysis and design were iterated to arrive at a configuration that meets the design requirements.

INTRODUCTION

The Martian Rover is part of the Mars Rover and Sample Return mission (MRSR) under study at the Jet Propulsion Laboratory (JPL) for the National Aeronautics and Space Administration. At JPL's request, the Department of Energy's Office of Special Applications commissioned Fairchild to perform a design study of RTGs to power the Rover.

Two companion papers presented at this conference described various RTG designs [1] and their thermal, thermoelectric, electrical, and mass analyses [2]. The present paper describes the structural design and analysis of those RTGs.

All RTG designs generated in the Fairchild study employ the General Purpose Heat Source (GPHS) module as the basic heat source building block. Each GPHS module produces 250 watts(t), and as many as 18 stacked modules are contained in each RTG. As shown in Figure 1, each module is contained in a graphite aeroshell, with outer dimensions of 3.8 by 3.7 by 2.1 inches. The aeroshell serves as the structural member of the heat source module. The inner components contribute to the GPHS mass and the inertial forces, but play no significant structural role.

Figure 1. General-Purpose Heat Source Module (250 Watt)

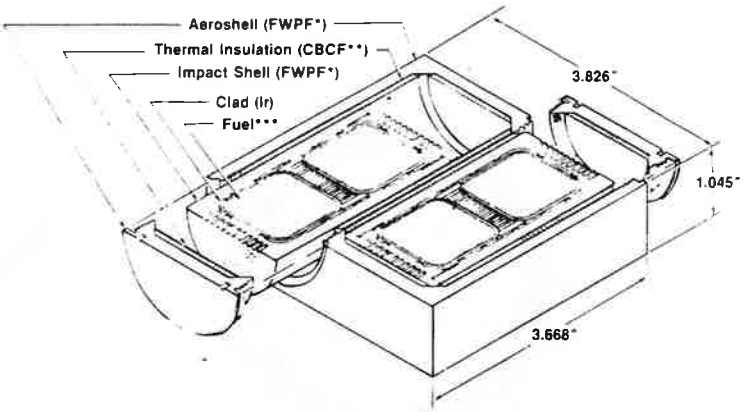

*Fine-Weave Pierced Fabric, a 90%-dense 3D carbon-carbon composite
**Carbon-Bonded Carbon Fibers, a 10%-dense high-temperature insulator
***62.5-watt $^{238}PuO_2$ pellet

The GPHS module design is primarily driven by safety considerations. The modules are designed to survive hypersonic reentry and subsequent Earth impact without fuel release. To maximize the impact safety margin, one wishes to minimize the impact velocity. Individual modules have a much lower impact velocity (49 m/s) than the stacked heat source (74 m/s). Therefore, it is desirable to support the heat source stack in such a manner that the individual modules separate during reentry. This is accomplished by structurally supporting the heat source stack from the RTG's aluminum housing, which melts during reentry, releasing the modules. But the same support structure must hold the stacked modules together during launch and operational vibration and shock loads.

The heat source support arrangement will be described in detail with respect to the baseline RTG design described in Reference [1]. That design contains 18 heat source modules and 576 thermoelectric unicouples, and produces 250 watts(e) at the end of the MRSR mission, based on demonstrated thermoelectric technology and measured performance levels.

Figure 2 shows horizontal and vertical cross-sections of the baseline RTG design. As indicated by the line C-C in the horizontal section, the left half of the vertical section represents a normal cut through the heat source stack, and the right half represents a diagonal cut. For the sake of clarity, only three of the eighteen modules are depicted in Section C-C. As indicated in that Section, there are two horizontal cuts. Section A-A shows a cut through the center of a heat source module, and Section B-B shows the upper heat source support structure. Both show a cut through a layer of thermoelectric unicouples, and through the RTG housing and radiator fins. The left half of Section C-C shows the length of the water-cooled RTG housing, and the right half shows its radiation-cooled length.

Figure 2. Baseline RTG Cross-Sections, Showing H.S. Structural Supports

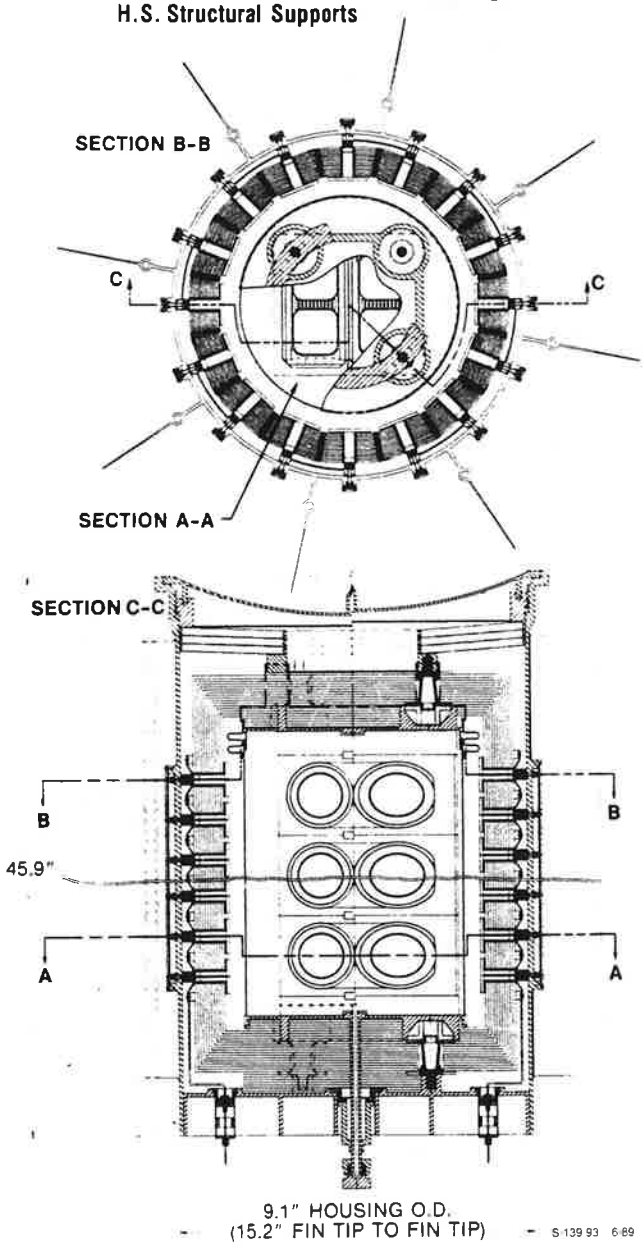

As shown, the heat source stack is only supported at its ends. There are no midspan supports. The heat source support structure is designed to hold the modules together under lateral loads of 25 G during Earth launch and 15 G during atmospheric entry, landing, and surface travel on Mars. This is done by using a set of Belleville springs to subject the stack to a large axial preload. The heat source canister serves only as a helium container. Its thin side wall plays no structural role.

Figures 3a and 3b present sectional trimetric closeups of the support structure at the top and bottom of the heat source stack. Figure 3a shows an exploded view of the upper structure, and Figure 3b shows the bottom structure, viewed from below. The multifoil thermal insulation has been omitted for clarity.

Figure 3a. Exploded View of Support Structure at Top of Heat Source

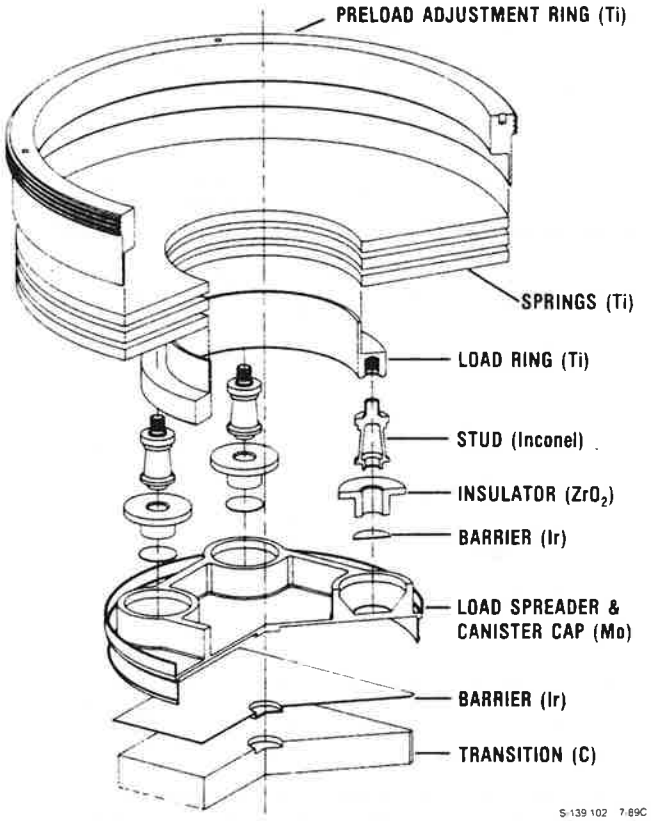

As shown, the first and last heat source modules are followed by graphite transition sections. Those transitions bear against the end caps of the molybdenum canister. Thin iridium sheets are used as reaction barriers between the graphite and the molybdenum.

On the outside of each of the canister end caps is a set of integral stiffening ribs and load stud seats. These form a square structure, to spread the axial load from the four load studs to the four edges of the heat source end face.

The axial load is applied by the four Inconel load studs via zirconia insulators, to reduce the axial heat losses and the load stud temperatures. As shown in Figure 2, the studs penetrate through the multifoil thermal insulation.

The upper set of load studs is bolted to a titanium load ring. As shown in Figure 3a, the axial preload force is applied to the load ring by a set of titanium Belleville springs, which bear against a preload adjustment ring that is threaded to the I.D. of the RTG's aluminum housing. After the load is set, the ring is prevented from backing off by anti-rotation pins.

The lower set of load studs is bolted directly to the baseplate of the RTG's aluminum housing, which has integral radial and circumferential stiffening ribs, as shown in Figure 3b.

Figure 3b. Exploded View of Support Structure at Bottom of Heat Source

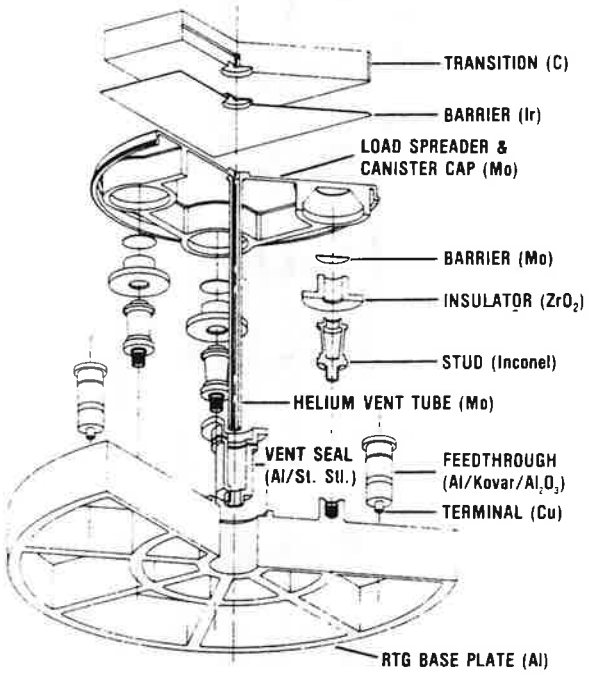

The structural design of the RTG consists of three principal tasks:

1. Determining how large a preload is required to hold the modules together during Earth launch and during Mars operations.

2. Designing the Belleville springs to supply the required spring force and spring travel.

3. Designing the RTG housing to withstand the bending moments on the cantilevered RTG during launch, to be structurally stable against the one-atmosphere external pressure, and to stay below the stresses where long-term creep would occur at the materials' operating temperatures.

These tasks are described in the next three sections.

DETERMINING THE REQUIRED PRELOAD FORCES AND RESULTANT GRAPHITE STRESSES

The heat source stack may be viewed as a partitioned beam with a distributed side load. If the beam were continuous rather than partitioned, the side load would produce axial compressive stresses on the side to which it is applied, and axial tensile stresses on the opposite side. But a partitioned beam cannot sustain a tensile stress in the axial direction. Therefore, in the absence of an axial preload, the side load would cause the partitioned beam to fall apart.

To hold the heat source stack together in the RTG, the axial preload must be high enough to equal or exceed the maximum tensile stress produced by the side load. When this principle was first applied [3], the authors mistakenly treated the GPHS module as though it were a solid block rather than a hollow box. This can lead to a serious overestimate of the required preload, as illustrated below.

Consider the simplified case of a hollow beam having a length **L** and cross-section bounded by an outer square of side **a** and concentric inner square of side **b**. The beam has fixed end supports and a uniform distributed side load **w** per unit length. Its maximum bending moment **M**, which occurs at the beam's ends and at its center, is given by

$$M = w L^2 / 24 . \qquad (1)$$

Its maximum tensile stress σ is given by

$$\sigma = M c / I , \qquad (2)$$

where **c** is the distance from the center to the outer fiber,

$$c = a / 2 , \qquad (3)$$

and **I** is the cross-section's moment of inertia, given by

$$I = (a^4 - b^4) / 12 . \qquad (4)$$

If the beam is partitioned (i.e., an unbonded stack), it will hold together if the compressive stress produced by the preload P equals the tensile stress σ. Hence,

$$P = \sigma(a^2 - b^2) , \qquad (5)$$

Combining Equations (1) through (5), we obtain the formula

$$P = \frac{w L^2}{4a\left[1 + (b/a)^2\right]} \qquad (6)$$

for the required preload P.

Clearly, increasing the size of the cavity in the hollow beam decreases the required preload. Equation (6) shows that in the limit, as **b** approaches **a**, the required preload for the hollow beam is only half as large as that for a solid beam **(b=0)**. This principle had been overlooked in Reference [3], but was recognized by Mr. Hamrick during the present study. It can make the difference between requiring or not requiring a midspan support.

The above derivation was for the idealized case of a simple hollow box beam. The modular heat source stack is more complicated. As shown in Figure 1, each module has top and bottom covers, and a curved cavity resulting in non-uniform side walls. To determine the required preload for such a modular stack, a detailed NASTRAN analysis was carried out, employing three-dimensional models of the modules' aeroshells and orthotropic properties of the carbon-carbon composite.

Figure 4 shows the undeformed grid model for half of the aeroshell of a single module. This and subsequent figures are sectioned at the plane of symmetry, the y-z plane. The appropriate number of such models were stacked up, linked to each other, and combined with models of the heat source support structure. The integrated model was then subjected to the axial spring load and to a side load of 25 G.

Figure 4. Nastran Model of GPHS Aeroshell

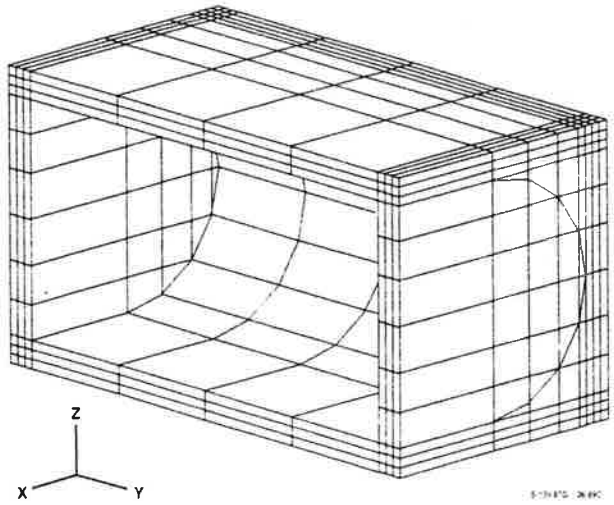

For a preliminary analysis, the heat source stack was analyzed without the effect of the simultaneous deformation of the cantilevered RTG housing. This simplification cuts the problem in half, because it results in identical end supports and symmetry about the heat source's midplane. Therefore, only half the heat source modules need to be modeled.

At the time of the preliminary analysis, we were considering a heat source of 16 instead of 18 modules. Therefore, our preliminary-analysis model consisted of eight heat source modules. The 16-module stack was subjected to a 4000-lb axial preload. The resultant deformation of the upper half of the 16-module stack is shown in Figure 5.

Figure 5. Deformation of Upper Half of Heat Source Stack Under 4000-lb Axial Load and 25G Side Load (Y)

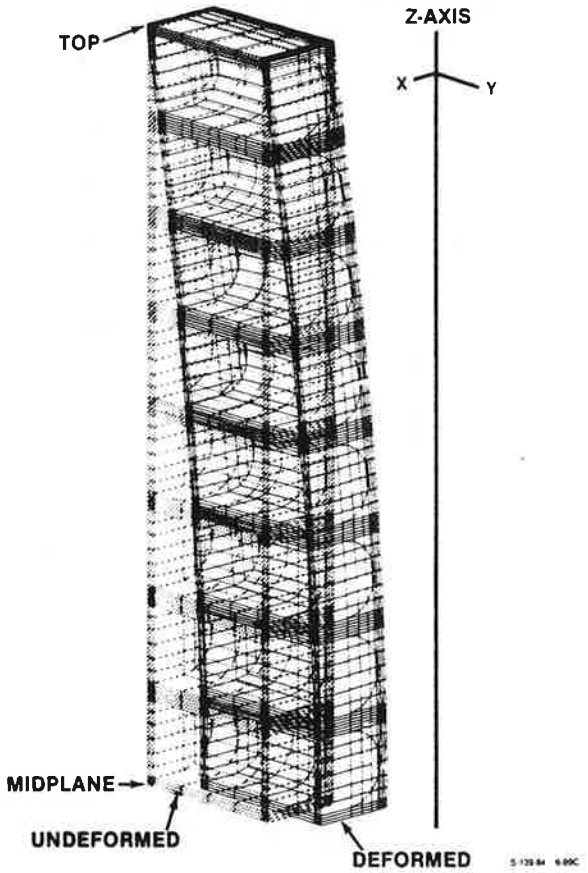

Figure 6 shows the normal Z-stresses in the first and eighth heat source modules. As can be seen, all Z-stresses are negative (i.e., compressive) except for one small section in the upper left corner of Module #1, which shows a tensile stress of 0.53 ksi. It was therefore concluded that the basic principle illustrated by Eq. (6) had been confirmed, but that the predicted 4000-lb preload is slightly inadequate for the 16-module heat source. Based on these results, it was decided to use a 5500-lb preload for the 18-module heat source in subsequent analyses.

Figure 6. Normal Z-Stresses in End and Center GPHS Modules

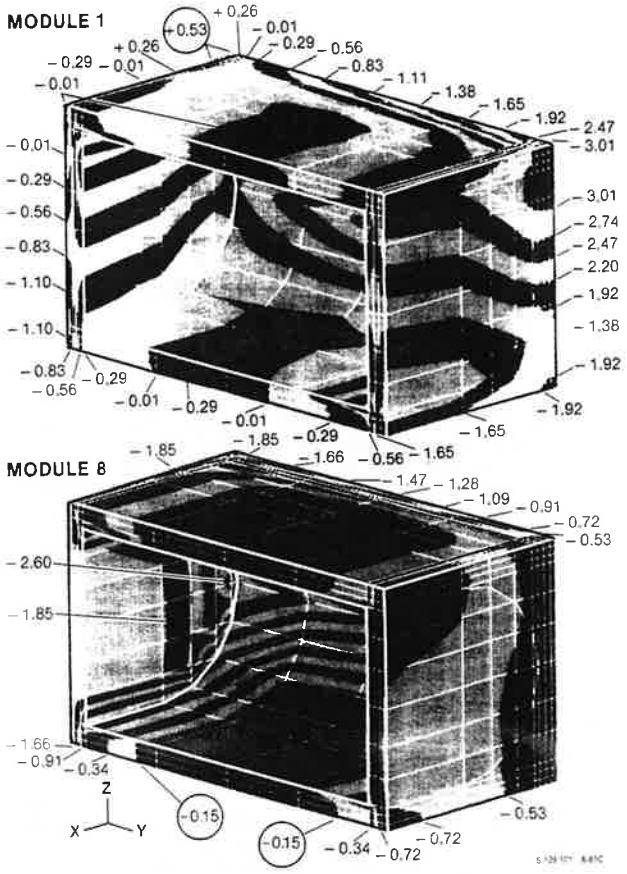

The same analytical model was used to compute the von Mises stresses in Modules 1 through 8. The maximum was found to occur in Module 1. Figure 7 shows the von Mises stresses in that module.

Figure 7. Von Mises Stresses in Module 1

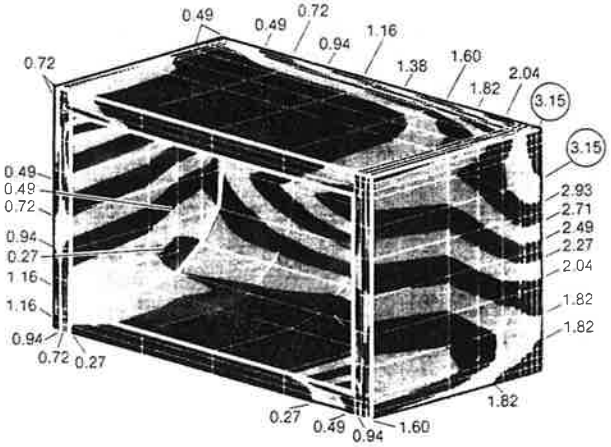

As can be seen, the maximum von Mises stress, in the upper right corner or Module #1, is 3.15 ksi. This is well within the tensile and compressive strengths of the Fine-Weave Pierced Fabric (FWPF) graphite material, as shown in Table 1, which was supplied by its manufacturer AVCO.

Table 1. Composite Strength (ksi) of AVCO Fine-Weave Pierced Fabric

TEMPERATURE	°F	75	600	1000	2000	3000	4000	5000
	°C	24	316	537	1093	1649	2204	2760
TENSION	Y	17.74	19.66	20.66	23.86	26.21	27.39	25.20
	X	17.64	19.66	20.66	23.86	26.21	27.38	25.20
	Z	18.17	20.24	21.28	24.57	26.99	28.20	25.95
COMPRESSION	Y	20.61	20.78	20.85	21.59	23.56	26.49	30.61
	X	20.61	20.78	20.85	21.59	23.56	26.49	30.61
	Z	20.8	21.0	21.11	21.89	23.89	26.66	31.00
SHEAR	YZ	1.17	1.11	1.07	1.00	0.99	1.26	1.00
	ZX	1.17	1.11	1.07	1.00	0.99	1.26	1.00
	XY	1.17	1.11	1.07	1.00	0.99	1.26	1.00

Table 1 shows that FWPF is much weaker in shear than in tension or compression. Therefore, the xy, xz, and yz shear stresses were computed, and found to be a maximum in Module 1. The three sets of shear stresses in that module are shown in Figure 8. The maximum shear stress of 0.138 ksi is only 14% of the material's shear strength, as shown in Table 1.

Figure 8. Module-1 Shear Stresses, in ksi

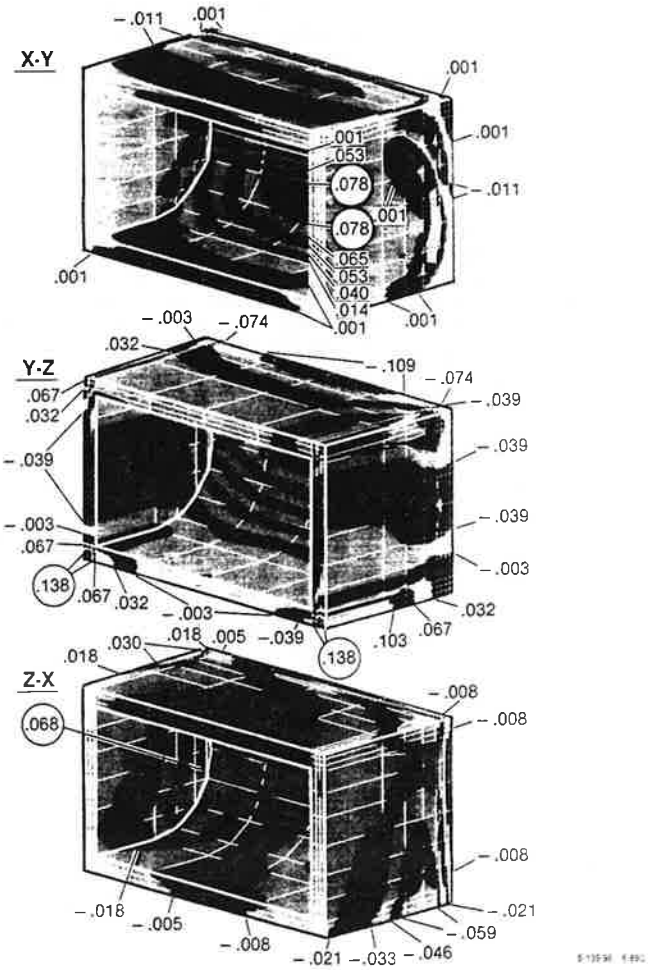

DESIGNING THE BELLEVILLE SPRINGS

The Mars Rover RTG design differs from other RTGs in that a preload is required not just for a brief period during Earth launch, but also during atmospheric entry and landing on Mars and during Rover activities on Mars for the full four-year duration of the MRSR mission. Although the G-loads during these post-launch operations (15 G) are lower than during launch (25 G), one cannot assume that springs which satisfy the higher requirement will automatically satisfy the lower. This is so because the Rover RTG is water-cooled during Earth launch and radiation-cooled during and after Mars landing, as explained in Reference [1].

In switching from water-cooling to radiation-cooling, the RTG's housing temperature rises by about 100°C, causing its length to grow by about 0.1". Since the thermal expansion of the graphite heat source is virtually negligible, the thermal growth of the aluminum housing causes a corresponding expansion of the Belleville preload springs, and consequently a relaxation of the compressive load on the heat source stack.

Therefore, the designer must consider the adequacy of the spring force both during launch and during subsequent Martian operations, at their respective RTG temperatures. At the same time, he must make certain that the maximum stress in the spring material under maximum-load conditions does not exceed the spring material's strength at temperature. Thus, the spring design must satisfy three independent constraints.

Consider a set of N_S x N_p conical (Belleville) springs of outer diameter D_o, inner diameter D_i, and thickness T. The spring set is arranged with N_p springs in parallel (i.e. nested) and N_S in series (i.e., stacked). The springs are made of a material with elastic modulus E and Poisson's ration μ. The overall free height of each spring is $H + T$. The deflection of each spring from its free height during Earth launch is Y_e. During Martian operations, the deflection of each spring from its free length is given by

$$Y_m = Y_e - \delta/N_s , \qquad (7)$$

where δ is the thermal growth of the aluminum housing length due to the change from water cooling to radiation cooling.

The load P_e exerted by the set of springs during Earth launch is given by [4]

$$P_e = \frac{N_p E Y_e \left[(H - Y_e/2)(H - Y_e) T + T^3\right]}{(1-\mu^2) C_0 (D_o/2)^2} , \qquad (8)$$

the corresponding load P_m during Martian operations is given by

$$P_m = \frac{N_p E Y_m \left[(H - Y_m/2)(H - Y_m) T + T^3\right]}{(1-\mu^2) C_0 (D_o/2)^2} , \qquad (9)$$

and the maximum stress σ (at the inner diameter of the springs) is given by

$$\sigma = \frac{E Y_e \left[C_1 (H - Y_e/2) + C_2 T\right]}{(1-\mu^2) C_0 (D_o/2)^2} , \qquad (10)$$

where C_0, C_1 and C_2 are dimensionless geometric constants defined by

$$C_0 \equiv \frac{6 (1 - D_i/D_o)^2}{\pi \ln(D_o/D_i)} , \qquad (11)$$

$$C_1 \equiv \frac{6}{\pi \ln(D_o/D_i)} \left[\frac{D_o/D_i - 1}{\ln(D_o/D_i)} - 1 \right] , \quad \textit{and} \qquad (12)$$

$$C_2 \equiv \frac{3 (D_o/D_i - 1)}{\pi \ln(D_o/D_i)} , \qquad (13)$$

Thus, given the values of N_p, N_S, D_o, D_i, P_e, P_m and δ, the spring design problem comes down to solving the three equations (8, 9, and 10) for the unknown spring dimensions T, H, and Y_e. Since these are simultaneous cubic equations, a trial-and-error solution is required. This was implemented by means of a Fairchild-generated computer program. The parameters used in the computations for the 18-module baseline RTG are summarized below:

$E = 11 \times 10^6$ psi	$\delta = 0.100$ in
$\mu = 0.31$	$\sigma = 82$ ksi
$P_e = 5500$ lb	$D_o = 8.75$ in
$P_m = 3300$ lb	$D_i = 3.20$ in

The spring's outer diameter D_o is designed to mate with the I.D. of the RTG housing, and its inner diameter D_i is designed to mate with the load ring to which the heat source support studs are bolted. Thus, the springs act as the radial support of the top of the heat source. (See Figure 2). To retain this benefit, an odd number was always picked for N_S, the number of springs (or nested springs) in series. Thus, the spring set is always loaded on the O.D. at the top and on the I.D. at the bottom.

For a given set of spring parameters, various combinations of N_S and N_p were tested. For some combinations, it was found that no physically real solution exists. But in general, there were several different combinations of N_S and N_p which satisfied the three equations and therefore the three constraints. For example, for the above parameters the equations are satisfied by the alternative solutions listed in Table 2.

Table 2. Spring Design Options Satisfying the Constraints on P_E, P_M, and σ

N_S	1	1	1	3	3	3	3	
N_P	3	4	5	1	2	3	4	
T	.221	.139	.088	.153	.061	.038	.028	inch
H	.230	.357	.414	.792	.896	.921	.933	inch
Y_E	.176	.161	.163	.076	.077	.077	.077	inch
Y_M	.076	.061	.063	.043	.044	.044	.044	inch

Each of the options listed in the table yields a preload of 5500 lbs on Earth, 3300 lbs on Mars, and a maximum stress of 82 ksi at the spring's I.D. Thus, any one of these options could be adopted. However, we preferred a single set of nested springs to a multiple stack, because it leads to a simpler and more compact RTG design.

Among the solutions for $N_s = 1$, we selected the one with the least number of springs, $N_s = 3$. Note that there is no physically real solution for $N_s = 1$ and $N_p = 1$ or 2. Thus, the spring design for the baseline RTG consists of three nested springs, with each spring having a thickness T of 0.221", a free height $H + T$ of 0.451", and a compressed height ($H + T - Y_e$) of 0.275" during Earth launch and ($H + T - Y_m$) of 0.375" during Mars operations.

DEFORMATION AND STRESSES WITH HEAT SOURCE SUPPORTED BY CANTILEVERED RTG HOUSING

The preliminary structural analysis described thus far employed a simplified analytical model. The model did not include the RTG housing, which supports the load springs that compress the heat source stack. Instead, the load springs were assumed to have symmetrical fixed-end supports. Because of that symmetry, only half the heat source stack needed to be modeled.

The more complete analysis described in this section does not employ these simplifications. The heat source is supported by the deformable RTG housing. Specifically, the upper springs are connected to the top of the housing side wall, and the lower heat source support studs are mounted on the housing baseplate.

The model of the housing includes the fin roots and cooling ducts which act as stiffeners. It also includes the radial and circumferential stiffeners of the baseplate. The housing is cantilevered, with only the rim of its baseplate fixed, and the rest of the housing free to lean away from the 25 G side load. The resultant angular deflection of the RTG's upper end results in highly unsymmetrical heat source supports. Therefore, it was necessary to model the whole 18-module heat source.

The solids model used for the preliminary analysis of the eight-module half-stack had 10,961 grid points and 26,652 degrees of freedom. Using a similar solids model for the full eighteen-module heat source would have exceeded the available computer time and disk space. To avoid that, the solids model was replaced with a plate model having an equivalent stiffness matrix. Even so, a very large (2140-node) NASTRAN model with 10,611 degrees of freedom was required to represent the heat source, its support structure, and the RTG housing.

Figure 9 depicts the model of the RTG in its undeformed and deformed shapes. The deformation shown includes the effects of the 25-G side load and of the 5500-lb spring force, which produces a compressive load on the heat source stack and a tensile load on the housing. The deformations shown have, of course, been exaggerated for improved visibility. Note the leaning of the housing and the bowing of the heat source in the y-direction, the axial elongation of the housing due to its tensile load, and the outbowing of the RTG's baseplate due to the downward force exerted by the heat source.

Figure 9. Deformation of Spring-Loaded Heat Source Supported by Cantilevered RTG Housing

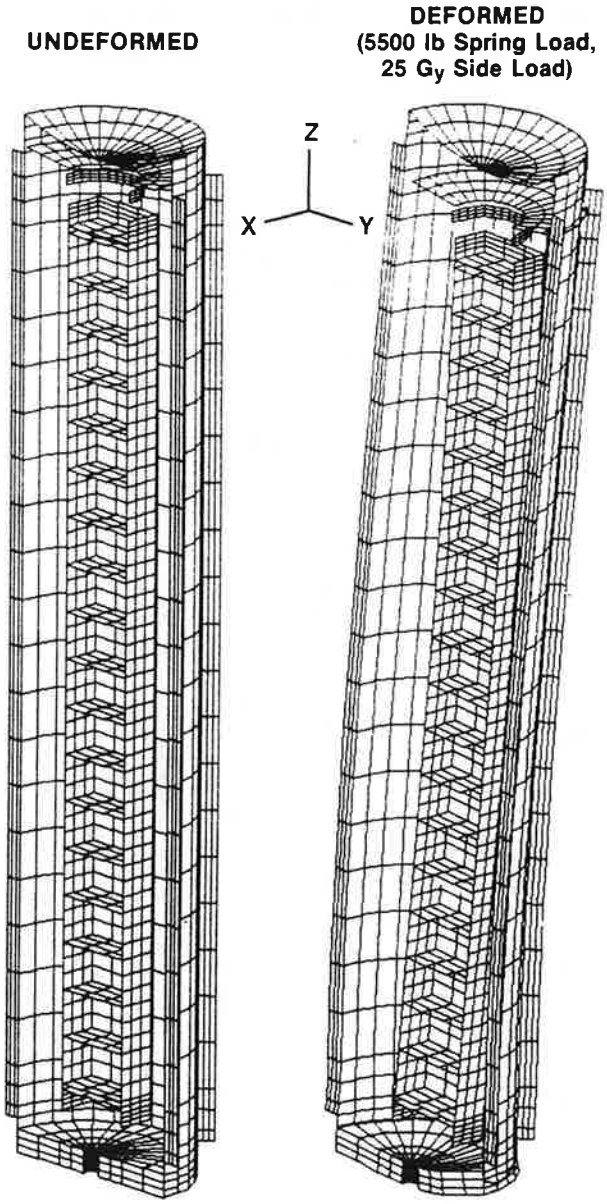

Figure 10 presents the normal-z stresses and von Mises stresses in the heat source side walls. As can be seen, all of the normal-z stresses are negative. The highest (i.e., least negative) z-stress is -1.09 ksi, well within the compressive regime. The computed results suggest that the 5500-lb preload can probably be reduced to 5000 lbs without developing any tensile z-stresses. The right half of the figure shows that the maximum von Mises stress, 2.9 ksi, is again well within the strength limit of the FWPF graphite material. (See Table 1.)

Figure 11 depicts the corresponding von Mises stress distribution in the RTG housing side wall. Two conditions are illustrated: The left half of the figure shows the short-term launch stresses of the water-cooled RTG housing with a 5500 lb spring load and a 25 G side load. The right half of the figure shows the long-term stresses of the radiation-cooled RTG with a 3300 lb spring load and a 15 G side load.

The maximum launch stress, which occurs at the -y side near the base of the RTG, is -15 ksi. This is well below the 31-ksi yield strength of the aluminum alloy (2219 T851) at its 171°C launch temperature. Similarly, the maximum stress on Mars, 8.5 ksi, is only 53% of the alloy's 16 ksi yield strength at its 272°C maximum operating temperature.

Figure 10. Stresses in Heat Source Aeroshells (ksi)

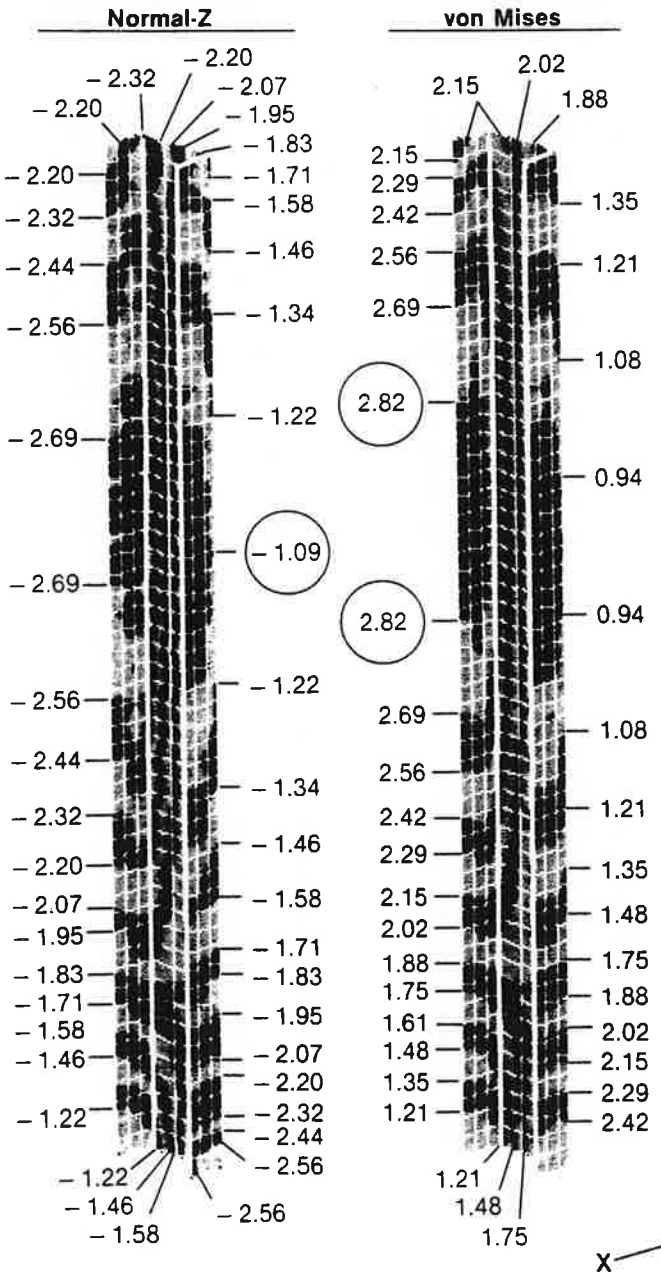

Figure 11. Von Mises Stresses in Housing Side Wall (ksi)

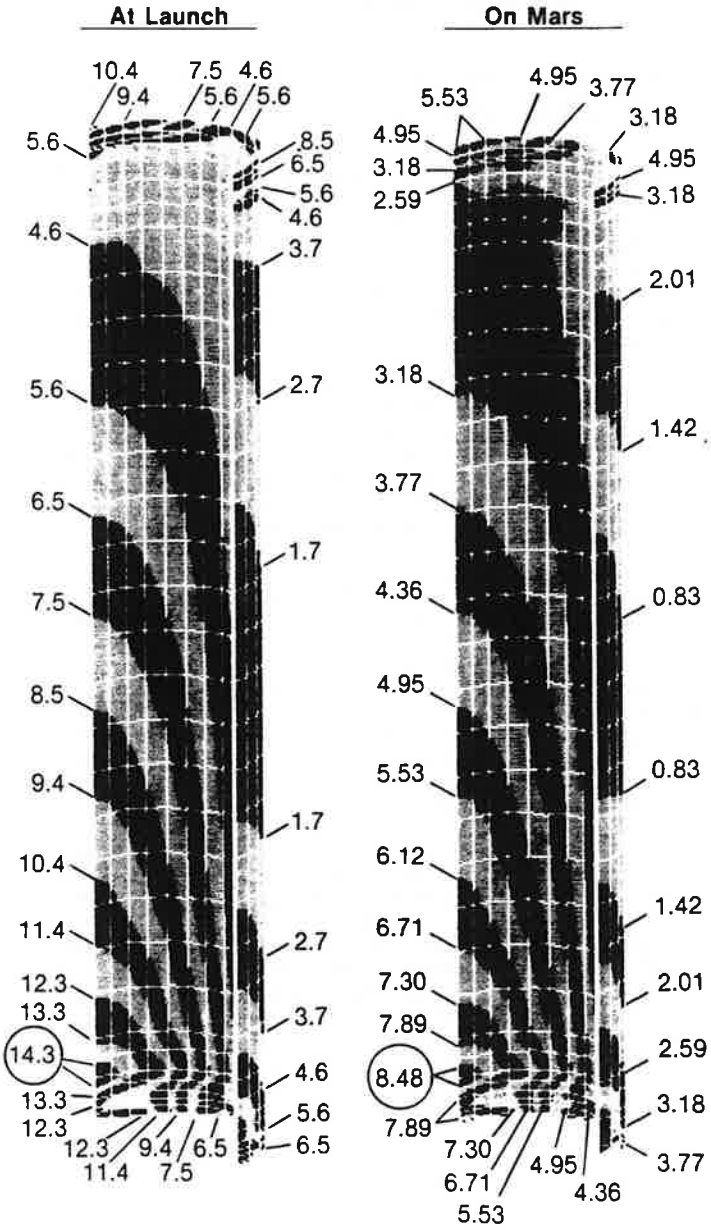

In addition to yield strength, the long-term creep characteristics of the aluminum housing must be considered. The RTG housing, at its thinnest (0.090") section, has a horizontal cross-section of 2.54 in^2. Thus, at its maximum operating temperature, the 3300-lb spring load will produce a steady-state tensile stress of 1.3 ksi. At 272°C, this tensile stress will produce negligible creep during the four-year mission.

Finally, Figure 12 shows the von Mises stress distributions in the RTG's 0.062"-thick top cap and in its 0.125"-thick baseplate. The top cap is subjected to an external pressure of one atmosphere. Its maximum stress, ~5 ksi, is well below the strength of aluminum.

Figure 12. Von Mises Stresses in RTG Top Cover and Base Plate

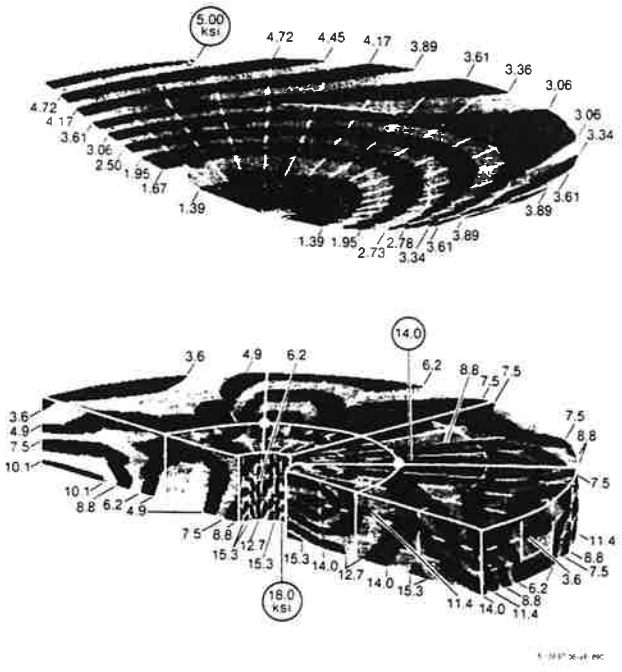

The heavy white lines in the baseplate stress plot show the location of the eight radial and three circumferential stiffening ribs, which are 0.25" thick and 1" high. The two white dots in the figure denote the locations of the heat source support studs. As can be seen, the maximum stress (18 ksi) occurs at the +y side of the inner stiffening ring. A secondary maximum (14 ksi) occurs at the right side of the middle stiffener ring. This location is directly below one of the two support studs at the +y side of the heat source. The maximum baseplate stress is is 42% below the 31-ksi yield strength of the aluminum alloy at its 171°C launch temperature.

SUMMARY AND CONCLUSIONS

Detailed NASTRAN analysis of the spring-loaded heat source supported by the cantilevered RTG housing confirms the feasibility of supporting an 18-module heat source stack without midspan supports, and demonstrates the adequacy of the spring and housing dimensions on which the mass analyses in Reference [2] are based.

REFERENCES

[1] A. Schock, V. Sankarankandath, and M. Shirbacheh, "Requirements and Designs for Mars Rover RTGs." 24th Intersociety Energy Conversion Engineering Conference, 6-11 August, 1989.

[2] A. Schock, T. Or and E. Skrabek, "Thermal and Electrical Analysis of Mars Rover RTGs." 24th Intersociety Energy Conversion Engineering Conference, 6-11 August, 1989.

[3] A. Schock and A. Shostak. "Use of Modular Heat Source Stack in RTGs." Proceedings of the 1979 Intersociety Energy Conversion Engineering Conference, Boston, MA.

[4] A. Hall Jr., A. Holowenko, and H. Laughlin, "Schaum's Outline of Theory and Problems of Machine Design." New York: McGraw-Hill Book Company, 1980.

ACKNOWLEDGEMENT

The above work was supported by the U.S. Department of Energy's Office of Special Applications.